MODIFICATION OF ELECTRODES MATERIAL IN A MICROBIAL FUEL CELL (MFC) TO ENHANCE THE ELECTRICITY PRODUCTION

BY

ANDIKA WAHYU AFRIANTO

A THESIS SUBMITTED IN PARTIAL FULFILLMENT OF THE REQUIREMENTS FOR THE DEGREE OF MASTER OF SCIENCE (ENGINEERING AND TECHNOLOGY)
SIRINDHORN INTERNATIONAL INSTITUTE OF TECHNOLOGY
THAMMASAT UNIVERSITY
ACADEMIC YEAR 2023

Ref. code: 25666422040920FRA

THAMMASAT UNIVERSITY

SIRINDHORN INTERNATIONAL INSTITUTE OF TECHNOLOGY

THESIS

BY

ANDIKA WAHYU AFRIANTO

MODIFICATION OF ELECTRODES MATERIAL IN A MICROBIAL FUEL CELL (MFC) TO ENHANCE THE ELECTRICITY PRODUCTION

was approved as partial fulfillment of the requirements for
the degree of Master of Science (Engineering and Technology)

on July 18, 2023

Chairperson _____
(Associate Professor Paiboon Sreearunothai, Ph.D.)

Member and Advisor _____
(Professor Sandhya Babel, D.Tech.Sc.)

Member _____
(Korakot Sombatmankhong, Ph.D.)

Director _____
(Professor Pruettha Nanakorn, D.Eng.)

Thesis Title	MODIFICATION OF ELECTRODES MATERIAL IN A MICROBIAL FUEL CELL (MFC) TO ENHANCE THE ELECTRICITY PRODUCTION
Author	Andika Wahyu Afrianto
Degree	Master of Science (Engineering and Technology)
Faculty/University	Sirindhorn International Institute of Technology/ Thammasat University
Thesis Advisor	Professor Sandhya Babel, D.Tech.Sc.
Academic Years	2023

ABSTRACT

The microbial fuel cell is a bioreactor that utilizes electroactive bacteria to manage pollutant levels in wastewater while simultaneously generating electricity. This technology has a very bright opportunity to develop and maximize its potential. Modification of activated carbon cloth (ACC) and carbon graphite electrode (GCE) with polyaniline (PANI) was carried out to improve the conductivity and biocompatibility properties of GCE and ACC. The modification was carried out by electrophoretic deposition (EPD) to coat the GCE and ACC surfaces with PANI. Characterization was carried out using FT-IR, FESEM, BET, and electrochemical analysis using cyclic voltammetry. The characterization results showed the presence of a porous structure on the electrode surface with an average particle size of 344,790.93 Å and 263.49 Å for GCE-PANI and ACC-PANI, respectively. The PANI structure was identified by the presence of a distinctive functional group, namely benzenoid (N–B–N) in the wave number region of around 1479 cm^{-1} and the quinoid group (N=Q=N) in the wave number region of approximately 1557 cm^{-1}. The results of the MFC operation gave the best results on the system with ferricyanide as the electron acceptor. The highest power density produced is 2.54×10^{-5} W cm^{-2} with a potential of 612.81 mV from MFC GCE-PANI and 1.65×10^{-8} W cm^{-2} with a

Ref. code: 25666422040920FRA

potential of 155.95 mV from MFC ACC-PANI. The normalized energy recovery of MFC GCE-PANI and ACC-PANI in ferricyanide is 0.115 kWh $kgCOD^{-1}$ and 5.67 × 10^{-3} kWh $kgCOD^{-1}$, respectively. The efficiency level of reducing COD levels reached 88.8% for MFC GCE-PANI and 87.2% for ACC-PANI.

Keywords: Microbial Fuel Cells, Graphite Carbon Electrode, Activated Carbon Cloth, Polyaniline, Electrophoretic Deposition

Ref. code: 25666422040920FRA

ACKNOWLEDGEMENTS

First of all, in the name of ﷲ, the praises to Him and the prophet Muhammad ﷺ. I am exceedingly grateful to be a master's student at the Sirindhorn International Institute of Technology (SIIT) at Thammasat University.

Second and foremost, I would like to express my sincere gratitude to my advisor, Prof. Dr. Sandhya Babel, for providing me with this opportunity to pursue my master's degree by joining her research team. Her guidance, support, motivation, and encouragement throughout my period in Thailand helped me improve my skills and knowledge to perform well in my studies and finish my research. Furthermore, I would also like to express my high appreciation to all my committee members, Assoc. Prof. Dr. Paiboon Sreearunothai and Dr. Korakot Sombatmankhong, for all their invaluable advice and support of my research.

Third, the highest gratitude is given to the Joint Graduate School of Energy and Environment at King Mongkut's University of Technology Thonburi (JGSEE-KMUTT). This study and research would not have been possible without the financial grant and support from the JGSEE Scholarship, which provided me with the joint master's degree program between JGSEE in KMUTT and SIIT at Thammasat University.

Moreover, I would also like to express a million thanks to all the laboratory technicians at the School of Bio-Chemical Engineering and Technology (BCET), all my labmates in the BCET's laboratory, all my research fellows in Prof. Babel's research group, and all the Indonesians in Thammasat University for all their help, motivations, and kindness to me during in this campus. Thank you for providing me with such a supportive environment to grow up and survive here.

Finally, my uncounted gratitude to my family, especially my parents, Mr. Parjimin Kartopawiro and Mrs. Sugirah Irianti Kartopawiro, who always became my supporters and believed me every time and everywhere I am. I dedicate this thesis to them with love.

Andika Wahyu Afrianto

Ref. code: 25666422040920FRA

TABLE OF CONTENTS

	Page
ABSTRACT	(1)
ACKNOWLEDGEMENTS	(3)
LIST OF TABLES	(7)
LIST OF FIGURES	(8)
LIST OF SYMBOLS/ABBREVIATIONS	(10)
CHAPTER 1 INTRODUCTION	1
1.1 Introduction and Problem Statement	1
1.2 Research Objectives	4
1.3 Scope of Research	4
CHAPTER 2 REVIEW OF LITERATURE	6
2.1 Microbial Fuel Cells System	6
2.2 MFC Designs	8
2.3 MFC Electrodes	10
2.3.1 Cathodic System	10
2.3.2 Anodic System	14
2.4 Modification of Electrode Materials	16
2.4.1 Modification of Carbon-Based Electrode Materials	16
2.4.2 Modification of Polymer-Based Electrode Materials	18
2.5 Polyaniline (PANI)	20
CHAPTER 3 Methodology	22
3.1 Preparation of Polyaniline (PANI)	22
3.2 Modification of Electrode Materials	22
3.2.1 Preparation of Aniline Monomer Solution	22
3.2.2 Electropolymerization on Graphite Carbon Electrodes (GCE)	22

Ref. code: 25666422040920FRA

3.2.3 Eleectropolymerization on Activated Carbon Cloth (ACC) 23
3.2.4 Eleectropolymerization on Activated Carbon Cloth-Carbon Tape (ACC-CT) 23
3.3 Characterization of Modified Electrodes 24
3.3.1 FTIR Characterization 24
3.3.2 FESEM Characterization 24
3.3.3 BET (Brunauer, Emmett, and Teller) Characterization 24
3.3.4 Cyclic Voltametry Analysis 26
3.4 Wastewater Preparation 26
3.4.1 The UASB Sludge Sampling 26
3.4.2 Preparation of Trace Nutrient 27
3.4.3 Synthesis of Artificial Wastewater 27
3.5 Configuration of MFC 28
3.6 Operation of MFC 29
3.7 Chemical Oxygen Demand (COD) Analysis 31
3.7.1 Preparation of Digestion Solution $K_2Cr_2O_7$ 0.1 N 31
3.7.2 Preparation of Sulphuric Acid 31
3.7.3 Preparation of Ferroine Indicator 31
3.7.4 Preparation of Ferrous Ammonium Sulfate (FAS) 0.05 N 31
3.7.5 COD Test and Calculation 32
3.7.6 Wastewater Treatment Efficiencies 32
3.8 Sludge and Wastewater Control During and After Experiments 33
3.9 Energy generation Analysis 33
3.9.1 Potential (V) 33
3.9.2 Current (I) 33
3.9.3 Current Density (I_d) and Power Density (P_d) 33
3.9.4 Normalized Energy Recovery (NER) and Current Efficiency (CE) 34
3.10 Salt Analysis 34
3.11 Flow Chart of Experiments 35

CHAPTER 4 RESULTS AND DISCUSSION 36
4.1 Synthesis of PANI 36

Ref. code: 25666422040920FRA

4.2 Electropolymerization of PANI 37
4.3 Modification of GCE 38
4.3.1 FTIR Analysis of GCE-PANI 38
4.3.2 SEM Analysis of GCE-PANI 39
4.3.3 BET Analysis of GCE-PANI 40
4.3.4 Electrochemical Analysis of GCE-PANI 41
4.4 Modification of ACC 43
4.4.1 FTIR Analysis of ACC-PANI 43
4.4.2 SEM Analysis of ACC-PANI 44
4.4.3 BET Analysis of ACC-PANI 45
4.4.4 Electrochemical Analysis of ACC-PANI 46
4.5 MFC Performances 47
4.5.1 Electricity Generation on MFC with Oxygen 48
4.5.2 Electricity Generation on MFC with Ferricyanide 53
4.6 Comparison of Electricity Generated in O_2 and $K_3[Fe(CN)_6]$ vs. Other Studies 56
4.7 Wastewater Analysis 57
4.7.1 Treatment Efficiencies 57
4.7.2 Normalized Energy Recovery (NER) and Current Efficiency (CE) 59
4.8 Salt Analysis and Identification 61

CHAPTER 5 CONCLUSION AND RECOMMENDATION 63
5.1 Conclusions 63
5.2 Recommendation 63

REFERENCES 65

APPENDICES 75
APPENDIX A 76
APPENDIX B 77
APPENDIX C 78

BIOGRAPHY 79

Ref. code: 25666422040920FRA

LIST OF TABLES

Tables	Page
2.1 Performances of carbon-based cathodes material in MFC system	11
2.2 Various types of carbon anode materials in MFC	16
2.3 Modification of several anode materials with carbon nanostructures	18
2.4 Types of anode modification with conducting polymers	19
2.5 FTIR characterization of PANI	21
4.1 The FTIR analysis and comparison between GCE and GCE-PANI	39
4.2 Surface characteristics of GCE and GCE-PANI	41
4.3 Surface characteristics of ACC and ACC-PANI	46
4.4 Operational duration of MFC with Oxygen	49
4.5 Power density and current density of MFC system with oxygen	52
4.6 Operational duration of MFC with $K_3[Fe(CN)_6]$	55
4.7 Power density and current density of MFC system with $K_3[Fe(CN)_6]$	55
4.8 COD removal efficiencies using with and without anode modification in MFC system	57
4.9 Comparison of COD removal of brewery wastewater treated in MFC	58
4.10 NERand CE of MFC in oxygen and ferricyanide systems	59
4.11 ICP analysis of oxidized salt on reactor surface	62

Ref. code: 25666422040920FRA

LIST OF FIGURES

Figures	Page
2.1 General principle of MFC (Kumar, 2016)	7
2.2 Single-chamber MFC	9
2.3 Dual-chamber MFC	10
2.4 Schematic representation of electrons transferred in two-chambered MFC	13
2.5 (a) carbon paper; (b) carbon cloth; (c) carbon mesh; (d) carbon felt; (e) graphite plate; (f) granular graphite; (g) reticulated verified carbon (RVC); and (h) carbon brush (source: Dumitru & Scott, 2016)	15
2.6 Structures of carbon nanostructures, (a) carbon nanotubes (CNTs); (b) graphene (G); (c) graphene oxide (GO); and (d) reduced graphene oxide (rGO).	17
2.7 Types of conductive polymers: (a) aniline monomer of polyaniline; (b) leucoemeraldine; (c) emeraldinebase; (d) emeraldine salt; (e) pernigraniline; (f) pyrrole monomer, and (g) polypyrrole	19
3.1 Illustration of EPD system	24
3.2 The illustration of the container to bring the UASB sludge	27
3.3 MFC reactor design	28
3.4 The MFC reactor	29
3.5 Diagram of the MFC with $K_3[Fe(CN)_6]$ as electron acceptor	30
3.6 Diagram of the MFC with oxygen as electron acceptor	30
3.7 Flow chart of experiments	35
4.1 FTIR spectra of PANI structure	36
4.2 Structure of PANI	37
4.3 Electrochemical particle coagulation on EPD coating process	37
4.4 GCE-PANI	38
4.5 Comparison of FTIR between unmodified GCE and GCE-PANI	38
4.6 FESEM micrographs of (a) GCE; and (b) GCE-PANI	40
4.7 N_2 adsorption/desorption curve of GCE anf GCE-PANI	40
4.8 The CV test of (a) GCE and (b) GCE-PANI	41
4.9 Comparison of CV test between GCE and GCE-PANI in each scan rates; (a) 25 mVs^{-1}, (b) 50 mVs^{-1}, (c) 100 mVs^{-1}, and (d) 200 mVs^{-1}	42

Ref. code: 25666422040920FRA

4.10 Specific capacitance of GCE vs. GCE-PANI 42
4.11 Unmodified ACC and ACC-PANI 43
4.12 Comparison of FTIR between unmodified ACC and ACC-PANI 44
4.13 FESEM micrographs of (a) ACC; and (b) ACC-PANI 44
4.14 N_2 adsorption/desorption curve of ACC and ACC-PANI 46
4.15 The CV test of (a) ACC and (b) ACC-PANI 47
4.16 Specific capacitance of GCE vs. GCE-PANI 47
4.17 Potential generated at 500 Ω resistor in O_2-based GCE MFC 48
4.18 Potential generated at 500 Ω resistor in O_2-based ACC MFC 49
4.19 Potential generated at 10,000 Ω resistor in O_2-based ACC-CT MFC 51
4.20 Polarization curve of: (a) Potential vs. External Resistor; and (b) Potential vs. Current Density 51
4.21 Current density vs. time between all electrodes at 500 Ω resistor with O_2 52
4.22 Potential generated at 500 Ω resistor in $K_3[Fe(CN)_6]$-based GCE MFC 53
4.23 Potential generated at 500 Ω resistor in $K_3[Fe(CN)_6]$-based ACC MFC 53
4.24 Current density vs. time between all electrodes at 500 Ω resistor with $K_3[Fe(CN)_6]$ 56
4.25 Salts on the surface of the anode chamber 62
A.1 Sludge sampling at Pathum Thani Brewery, Co., Ltd. 76
B.1 Experimental Models 77
C.1 MFC reactors setup in operational times 78

Ref. code: 25666422040920FRA

LIST OF SYMBOLS/ABBREVIATIONS

Symbols/Abbreviations	Terms
AC	Activated carbon
ACC	Activated carbon cloth
ACC-PANI	Activated carbon cloth-polyaniline
ACC-CT	Activated carbon cloth-carbon tape
ACC-CT/PANI	Activated carbon cloth-carbon tape/polyaniline
ATR	Attenuated total reflectance
BET	Brunauer–emmett–teller
BOD	Biological oxygen demand
CC	Carbon cloth
CE	Current Efficiency
CNT	Carbon nanotubes
COD	Chemical oxygen demand
CV	Cyclic Voltammetry
EDTA	Ethylenediamine tetra-acetic acid
EPD	Electrophoretic Deposition
FAS	Ferrous ammonium sulfate
FESEM	Field emission scanning electron microscopy
FTIR	Fourier transform infrared
GAC	Granular activated carbon
GCC	Graphene carbon cloth
GCE	Graphite carbon electrode
GCE-PANI	Gprahite carbon electrode-polyaniline
GFB	Graphite fiber brush
GO	Graphene oxide
MFC	Microbial fuel cell
NER	Normalized energy recovery
ORR	Oxygen reduction reactiom
PANI	Polyaniline
PEM	Proton exchange membrane

Ref. code: 25666422040920FRA

POAO	Poly(aniline-*co*-*o*-aminophenol)
rGO	Reduced graphene oxide
RVC	Reticulated verified carbon
SHE	Standard hydrogen electrode
UASB	Up-flow anaerobic sludge blanket

Ref. code: 25666422040920FRA

CHAPTER 1
INTRODUCTION

1.1 Introduction and Problem Statement

The bio-electrochemical devices known as microbial fuel cells (MFCs) use microbial activity to extract energy from wastewater while oxidizing organic molecules in the effluent. In MFCs, bacteria that have catalytic activity convert chemical energy to electricity. Microbial metabolism at the anode of an MFC can use extracellular electron transfer to transform the chemical energy in organic substances into electricity (Iftimie & Dumitru, 2019). MFCs are superior to other technologies due to many distinctive qualities. (i) MFCs are more effective than other types of batteries at converting chemical energy into electric current. (ii) Unlike other bioenergy technologies, MFCs may perform well throughout a wide temperature range (20 to 40 ^{o}C). (iii) Because the cathode may aerate passively, an MFC system does not require external power to aerate to deliver oxygen (as an electron acceptor) during operation. MFCs come in a variety of forms and materials. These systems are often operated in ideal conditions to produce more energy but can also work in other environments (Kumar et al., 2016).

MFC can generate electricity and treat wastewater simultaneously, potentially lowering wastewater treatment facility operating costs. As an environmental technology, MFC can lower certain aspects of environmental pollution. The parameters that are decreased in this system are chemical oxygen demand (COD) and biological oxygen demand (BOD) (Pant et al., 2010; Sun, 2016). The MFC system has been employed with various wastewater as a substrate, including liquid waste from households, chocolate factories, waste from beer factories (Wang et al., 2008), tempe industrial waste (Sudarlin et al., 2020), dairy industry waste (Faria et al., 2017), synthetic wastewater, and more. Organic matter digested by microbes in wastewater is generally sucrose and glucose (Pant et al., 2010). Because waste is cheap and easy to handle, producing electricity from wastewater oxidizing using MFC may offer a consistent and affordable solution for addressing environmental damage and energy shortages (Choudhury et al., 2017).

Ref. code: 25666422040920FRA

MFCs serve as reactors in which chemical energy is produced utilizing bacteria as a biocatalyst by oxidizing biodegradable substrates. The process underlying direct electron transmission is the formation of a biofilm on the anode surface. The high coulomb efficiency of this microorganism induces biofilm formation. The biofilms send electrons directly to the anode, acting as an electron acceptor. Because electrons flow straight, more energy is created, but it is still a tiny quantity. Another difficulty is that MFCs produce far less energy than chemical fuel cells (Santoro et al., 2017; Choudhury et al., 2017).

A proton exchange membrane (PEM) MFC reactor was built by Elakkiya and Matheswaran (2013) to handle liquid waste from the dairy industry. A dual-chamber reactor system uses the Nafion 117 PEM as its PEM. With the reduction of a COD level of almost 91%, this experiment generated a maximum power density of 192.161 mW/m^2. To treat dairy industry waste with a maximum COD removal of up to 63 5%, Faria et al. (2017) also performed PEM MFC with PEM Nafion 117 membrane by creating a dual-chamber reactor system and producing a power density of 92.2 mW/m^2.

Pottery-style ceramic MFC systems were examined by Tamakloe et al. (2015). The MFC's single-chamber reactor uses an earthenware membrane and anode chamber. Aluminium was the cathode's electrode, while a zinc rod was the anode. According to the findings, a reactor with a 1.7 L capacity produced a power density of 369 mW/m^2 and a reactor with a 1 L capacity at a rate of 55 mW/m^2. For its 1.7 L and 1 L capacities, respectively, this system removed COD at 86.9% and 88.1%.

Sejati and Sudarlin (2021) studied Tempe waste-based ceramic-based microbial fuel cells. The analyte in this investigation was tempe waste, the electrodes were made of graphite carbon, and the catholyte was $KMnO_4$. With COD and BOD elimination being 88.8% and 33.9%, respectively, the study's most significant power density gain is 1447.91 mW/m^2.

The problem of MFC technology is that MFC produces low power output. Several strategies to increase MFC power output include isolating particular microbial species, choosing organisms that produce mediators, or electrochemically enhancing the electrode surface (Pant et al., 2010). Maximizing power production of MFC requires optimization in both anode and cathode performances, model of the reactor

Ref. code: 25666422040920FRA

(such as the capacity and distances between two electrodes), chemicals, membrane for ion transfer, microbial species and their metabolisms, and operating condition (Rossi & Logan, 2021; Tamakloe et al., 2015). Electrode alteration is one of the many approaches to address this problem. The MFC performance can be significantly improved by changing the anodes. The surface properties of the anode material greatly influence the bacterial adhesion and electron transmission from the bacteria to the electrode. According to Iftimie and Dumitru (2019), it is possible to modify the anode surface with various functional groups with varying selectivities for specific bacteria to improve the transfer of electrons from bacteria to electrodes. The conducting polymers have good conductivity and electrochemical activity and can provide a suitable environment for bacteria (Mathew & Thomas, 2020).

Iftimie and Dumitru (2019) conducted research by modifying carbon nanotubes (CNT) using two methods. The first method involves using 4-nitroaniline, sodium nitrate, and concentrated HCl to modify CNT with nitrophenyl groups (CNT1). The second method involves the chemical reduction of 4-Nitrobenzenediazonium tetrafluoroborate with hypophosphorous acid as a reducing agent (CNT2). Lastly, CNT0 refers to an unmodified CNT. This study shows that CNT modification can increase the power density gain in the MFC system. CNT0 produces a power density of 145.2 mW/m^2 without modification, whereas the modified CNTs produce a higher power density by adding nitrophenyl groups. CNT1, with the addition of 4-nitroaniline, produces 296.1 mW/m^2, while the CNT2 with 4-Nitrobenzenediazonium tetrafluoroborate can produce a power density of around 393.8 mW/m^2. The addition and control of nitrogen groups on the electrode surface will improve MFC performance through electrode modification.

This research shows a new perspective to solve the low power generation in MFC technology. Carbon-based polymer coating anodes were synthesized to develop low-cost anode materials with high biocompatibility properties suitable for bacteria growth to enhance the power generated from MFC. In this study, the graphite carbon electrode (GCE) and activated carbon cloth (ACC) were coated with polyaniline (PANI) and used in the microbial fuel cell reactor with synthetic wastewater as the substrate. Instead of modifying one type of carbon material with PANI, this research coated PANI on two carbon materials to explain the effects of the differences between

two carbons' properties with resulting PANI layers. It can also show which carbon materials PANI works better as an anode to provide a suitable environment for growing electroactive bacteria.

1.2 Research Objectives

The performances of the microbial fuel cell reactor in decreasing waste pollutants and generating power were investigated in this study. This study offered a viable way to improve waste treatment efficiency and environmental friendliness while optimizing electrical energy derived from organic materials. The following are the specific suggested particular objectives:

1) To study the effects of PANI coating on the GCE and ACC anodes to generate electricity with MFC.
2) To study the influence of different electron acceptors in the performance of MFC.
3) To investigate the efficiency of MFC in wastewater treatment.

1.3 Scope of Research

Two lab-scale dual-chamber MFC reactors were constructed to meet the above objectives. The anodic chamber is filled with wastewater, while the cathodic chamber is an electrolyte solution. The MFCs were observed continuously in two cycles of operation. The following scopes are:

1) PANI coating deposited by the electrophoretic deposition method on the surface of GCE and ACC. The modified anodes are named GCE-PANI and ACC-PANI. The GCE-PANI and ACC-PANI were analyzed using the fourier transform infrared (FTIR), brunauer–emmett–teller (BET), field emission scanning electron microscopy (FESEM), and cyclic voltammetry (CV).
2) The GCE-PANI and ACC-PANI were applied in a microbial fuel cell reactor as an anode. The effectiveness of the modified and unmodified electrodes in generating electricity was compared in this study. The MFC circuit is connected to a data logger with a test period depending on two MFC start-up cycles. The capacity of the MFC reactor is 500 mL, with 250 mL of capacity

Ref. code: 25666422040920FRA

in each chamber. The electricity parameters observed are voltage generated, power density, and current density.

3) The MFCs operated with two types of electron acceptors. Oxygen and $K_3[Fe(CN)_6]$ were the electron acceptors in this research. The first system is constructed with a cathodic chamber filled with water and flows with oxygen aeration. The second system was constructed with a cathodic chamber filled with $K_3[Fe(CN)_6]$ 0.5 M.

4) The wastewater used in this research is synthetic wastewater containing 1000 mg/L COD with the addition of anaerobic bacterial inoculum from the brewery industry in Thailand, about 20% of the reactor's capacity. The wastewater parameter observed is chemical oxygen demand (COD) and Normalized Energy Recovery (NER).

Ref. code: 25666422040920FRA

CHAPTER 2
REVIEW OF LITERATURE

2.1 Microbial Fuel Cells System

MFC is a bioreactor that converts biomass into electricity through microorganisms electrochemically. Pant et al. (2010) state that the MFC produces electricity by converting chemical energy from microbial activity in wastewater. Redox reactions, which involve the oxidation of organic substances inside the anode and the reduction of molecules with more significant electrochemical potential at the cathode, are the basis for how MFCs work (Mook et al., 2013). In order to track electron mobility, a cable connecting two electrodes is used. The biodegradation of organic material yields electrical energy. For the most part, when wastewater is employed as a substrate, MFC is a potential long-term answer to meet rising energy demands (Iftimie & Dumitru, 2019).

Aelterman et al. (2006) stated that microorganisms serve as biocatalysts, transforming electron flow, such as chemical energy, into electricity. The MFC voltages are limited, while the maximum current is determined by (i) the model of an MFC reactor, such as single-chamber or dual-chamber. (ii) volumetric loading, which is the total amount of electrons delivered to produce the current, and (iii) the Coulombic efficiency (substrate converted into electricity).

An innovative approach to controlling wastewater sustainability is offered by MFC technology. Organic materials quickly oxidize in the anodic chamber and allow MFCs to be used for treating the wastewater. MFC systems have been used in various new applications in recent years, including seawater desalination, hydrogen generation, biosensors, and microbial electrosynthesis. As an environmental technology, MFC can reduce environmental pollution parameters such as chemical oxygen demand (COD) and biological oxygen demand (BOD) (Sun et al., 2016; Ucar et al., 2017). Ghadge and Ghangrekar (2015) explained that, as a result, the operation of the MFC system will be closely related to bacterial-based biological reactions, including glycolysis and electron transfer activities. To produce energy, the microbes in the MFC circuit serve as catalysts by oxidizing inorganic and organic substances. Microorganisms act as biological catalysts that can oxidize organic compounds in

Ref. code: 25666422040920FRA

electrolyte solutions and cause the flow of electrons from the anode to the cathode side.

To maintain a neutral charge, ions diffuse across the opposing membrane. This catalytic activity of microorganisms will decrease the parameters of waste pollutionThis catalytic activity of microorganisms will decrease the parameters of waste pollution, and the system will also produce power (Virdis et al., 2011). The illustration diagram of MFC principles is shown in Figure 2.1.

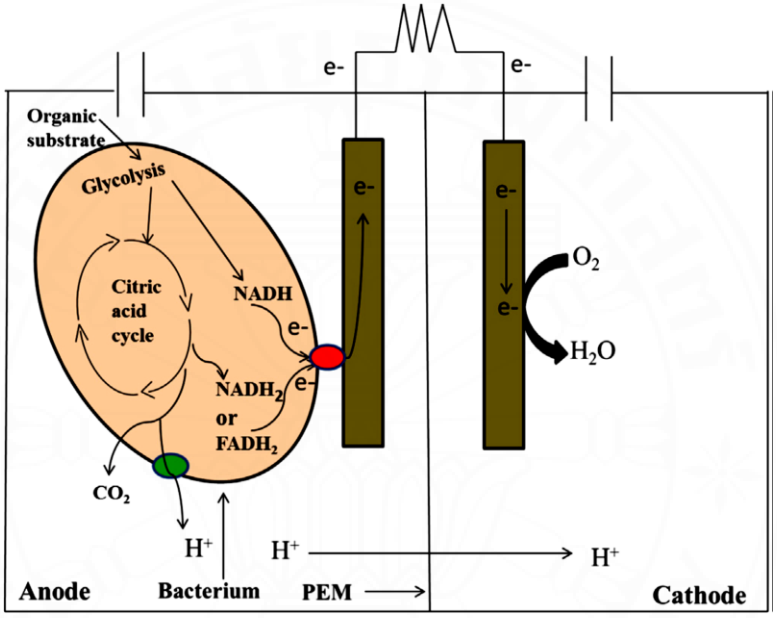

Figure 2.1 General principle of MFC (Kumar, 2016)

Pant et al. (2010) state that redox processes could connect the MFC to produce electrical energy. An anode oxidation method can be used with any biodegradable organic material. Sugars, organic acids like glucose and acetate, and complex polymers like starch and cellulose are used in MFC research. Equation 1 depicts the anode's response.

$$C_6H_{12}O_6 + 6H_2O \rightarrow 6CO_2 + 24H^+ + 24e^- \quad E^{o'} = -0.43\text{V vs. SHE at pH 7} \quad (2.1)$$

where standard redox potential is stated with $E^{o'}$ and the standard hydrogen electrode (SHE) is used to compare it.

The most apparent reaction at the cathode of MFCs is oxygen reduction owing to its excellent redox potential and quick availability in the air. The oxygen reduction reaction (ORR) is constrained because oxygen does not dissolve well in the

Ref. code: 25666422040920FRA

electrolyte. Other redox functional pairs for reactions at the cathode are hexacyanoferrate and Ferric/ferrocyanide. An increasingly positive redox potential characterizes the most practical cathode reaction for power production in MFCs (Rabaey et al.,2005; Logan et al., 2006). Equation 2.2 depicts the reaction of oxygen reduction,

$$O_2 + 4H^+ + 4e^- \rightarrow 2H_2O \quad E^{o'} = -0.82V \text{ vs. SHE at pH 7} \qquad (2.2)$$

The Nernst equation describes the potential of the equilibrium electrode (E_e) in an open circuit, which is affected by species concentration, pH, and temperature.

$$E_e = E^o + 2.303 \frac{RT}{nF} log \frac{C_o}{C_R} \qquad (2.3)$$

The R-value for the molar gas constant is 8.314 J/mol/K when the standard potential is represented in E_o. The sign *n* denotes the number of electrons exchanged. At the same time, the temperature is expressed in Kelvin with the symbol T. C_O and C_R are the concentrations of the oxidized and reduced products. At the same time, the Faraday constant, 96.485 C/mol, is represented in F. The difference between the cathode and anode equilibrium potentials is the basis for calculating the MFC cell potential. The MFC system, in which $E_{cathode} > E_{anode}$ results in the generation of electricity (Bajracharya et al., 2016).

2.2 MFC Designs

Several variations of MFC have been developed, including Single-Chamber, Dual-Chamber, and Stack MFC. "Single-chamber MFC" refers to a reactor constructed from only one chamber with mixed substrate and electrolyte solution. The liquid waste substrate is housed in the anode chamber of a dual-chamber MFC. In contrast, an electrolyte solution is present in the cathode chamber and is divided from it by a salt bridge or cation exchange membrane. One or more single- or dual-chamber MFC arranged in series, parallel, or series-parallel systems make up a stack MFC (Karmakar et al., 2010).

Ref. code: 25666422040920FRA

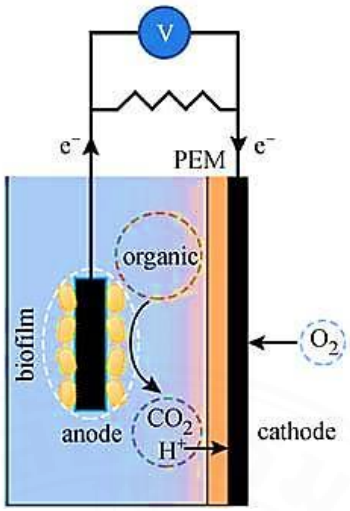

Figure 2.2 Single-chamber MFC

According to Windfield et al. (2016), the single-chamber MFC design with a cathode in direct contact with the air is appealing because it does not require the comparatively expensive PEM. A standard technology utilized in wastewater treatment techniques is the single-chamber MFC system. The MFC with a cathode in direct contact with the air is the type that is most likely to be scaled up in wastewater treatment due to the high energy production, straightforward design, and relatively low cost compared to other forms of MFC. Even though it may lower reactor expenses, eliminating this barrier has the drawback of causing oxygen diffusion to the anode.

The anode and cathode chambers are two MFC dual-chamber type vessel chambers. The PEM is sandwiched between the two chambers of the vessel, allowing the protons generated in the anode chamber to flow into the cathode chamber. The anode and cathode connect by titanium or copper wire. Microorganisms in the anode chamber will oxidize the organic waste substrate, producing electrons, protons, and carbon dioxide. Electrons generated by microbial metabolic activity are transferred to the anode surface by active redox proteins or cytochromes. They transfer through the electrical connection to the cathode. In the cathode space, there will be a reduction of electrons. Typically, oxygen or ferric chloride is the electron acceptor in the cathode chamber, where the electrons mix with protons and oxygen. A platinum catalyst can also facilitate this process (Kumar, 2016).

Ref. code: 25666422040920FRA

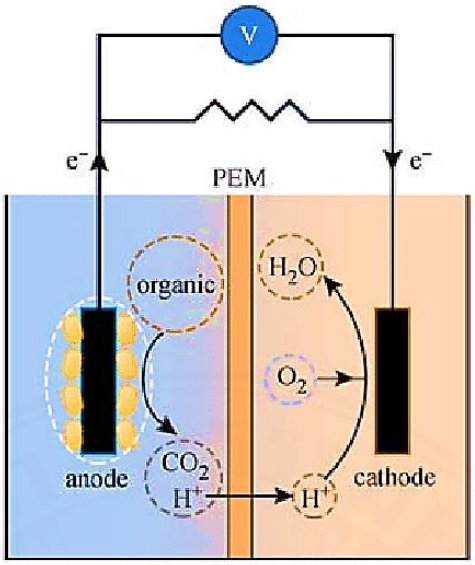

Figure 2.3 Dual-chamber MFC

2.3 MFC Electrodes

2.3.1 Cathodic System

The kind of substrate, exoelectrogenic bacteria, circuit resistance, electrode material, reactor arrangement, and electron acceptors all affect the MFC's power output. Distinct electron acceptors have different physical and chemical features that impact the efficiency of electricity production (Ucar et al., 2017).

The outcome potential is affected by the cathode substance. It is possible to use the cathode material as an anode as well. The efficiency of the MFC depends on anodic oxidation rather than a cathodic reduction because the reaction at the cathode will be constant (abiotic) regardless of changes in microbial metabolism at the anode; however, the more influential the cathode, the more significant the impact of the MFC in electricity production. An appropriate cathode is now needed for an efficient MFC design. One of the most challenging aspects of MFC technology is the cathode material and architecture. Carbon-based materials are the most commonly used electrodes for MFC cathodes. The attractive characteristics of carbon-based materials include excellent conductivity, low cost compared to other materials, and strong chemical stability and biocompatibility (Bajracharya et al., 2016).

An activated carbon cathode is a suitable electrode for non-catalyzed air cathode MFC due to its specific surface area and adsorption capacity. By adding

Ref. code: 25666422040920FRA

electron mediators into graphite electrodes, the electricity MFC generates may be multiplied by 1000 (Park & Zeikus, 2003). Table 2.1 shows the performances of carbon-based cathodes in MFC.

Table 2.1 Performances of carbon-based cathodes material in MFC system

Cathode Material	Catalyst	Catholyte	MFC Chamber Setup	MFC performance	Reference
CC	Pt	Phosphate buffer solution	Single	1.1 W/m^2	Ahn et al. (2014)
CC	MnO_2	Air	Dual	3.4 W/m^2	Kumar et al. (2014)
CC	MnO_2	Brewery	Single	0.02 W/m^2	Zhuang et al. (2009)
CC	Pt	Buffer saline	Triple	6.8 W/m^3	Zhang and He (2012)
AC	Ni	Air	Single	1.2 W/m^2	Cheng et al. (2014)
AC	-	Air	Dual	0.3 W/m^2	Deng et al. (2010)
GAC	-	Phosphate buffer solution	Dual	0.7 W/m^2	Zhang et al. (2013)
GAC	Biocathode	Buffer saline	Dual	24.3 W/m^3	Wei et al. (2011)
GFB	Biocathode	Buffer saline	Dual	68.4 W/m^3	You et al. (2009)
GC	-	Permanganate	Dual	1.447 W/m^2	Sejati and Sudarlin (2020)
GCC	-	Ferricyanide	Dual	0.199 W/m^2	Huang et al. (2021)

CC = carbon cloth; AC = activated carbon; GAC = granular activated carbon; GFB = graphite fiber brush; GC = graphite carbon; GCC = graphene carbon cloth

Table 2.1 shows the performances of several carbon-based cathodes. The data explained that the catalyst used could increase the power density production of the system. It compares activated carbon cathodes from Cheng et al. (2014) and Deng et al. (2010). The MFC system with activated carbon cathodes with catalyst Ni metal produced a higher power density than the non-catalyst activated carbon-based MFC.

Ref. code: 25666422040920FRA

However, a reactor system uses an electrolyte solution as a cathode. Two electrolyte cathodes that are frequently used in MFC systems are potassium permanganate ($KMnO_4$) (Sudarlin et al., 2020) and potassium ferricyanide ($K_3[Fe(CN)_6]$) (Elakkiya et al., 2013; Faria et al., 2017). The peroxide group, which can release oxygen during oxidation, and the high standard reduction potential of $KMnO_4$ make them suitable for use as MFC electrolyte cathodes. Due to its role as an electron acceptor in the MFC system, Logan (2006) examined $K_3[Fe(CN)_6]$'s application as an electrolyte cathode. $K_3[Fe(CN)_6]$ has a standard reduction potential of +0.36 and is a highly electroactive species that can capture electrons.

The performance of the MFC is significantly impacted by electron acceptors, which take in the electrons. Alternative electron acceptors offer the potential to increase power output, decrease operational costs, and increase the range of applications for MFCs. Now, some refractory materials can function as electron acceptors in the cathode. According to these findings, MFCs could control pollution (Ucar et al., 2017). The following electrolytes are some of those utilized in MFC as electron acceptors.

a) Oxygen

At the cathode, oxygen is frequently utilized as an electron acceptor. The reason is that oxygen has an excellent capacity for oxidation and creates a clean product in water (Strik et al., 2010). The electrons move towards the cathode through an external circuit in the MFC. The reaction that occurs between protons and oxygen will result in the creation of water.

$$O_2 + 4H^+ + 4e^- \rightarrow 2H_2O \qquad E^0 = 1.23\ V \qquad (2.4)$$

The potential for electrical generation is maintained by oxygen use, according to Equation (2.4). In order to provide oxygen to the cathode, an air cathode can be used; however, some disadvantages restrict the use of oxygen in MFCs, including the restricted interaction of oxygen with the electrodes and the slowly occurring oxygen reduction at typical carbon electrodes (Ucar et al., 2017).

Ref. code: 25666422040920FRA

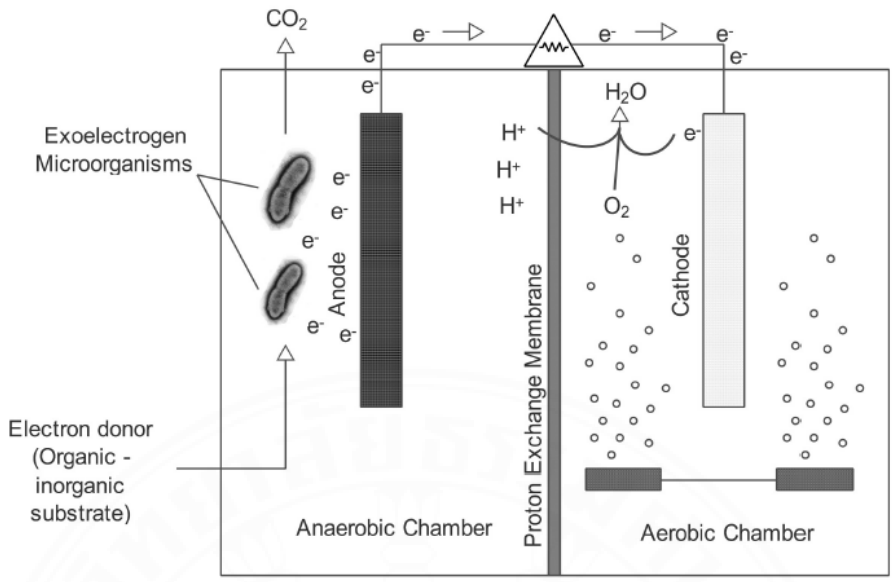

Figure 2.4 Schematic representation of electrons transferred in two-chambered MFC

b) Permanganate

In an atmosphere that is both acidic and basic, permanganate transforms into manganese dioxide by taking three electrons. Due to its properties, permanganate is a potential electron acceptor. Because of its more significant oxidation potential in acidic environments than alkaline ones, permanganate is expected to produce more power. As a result, a permanganate study in MFCs was carried out at various pH values (You et al., 2006).

$$MnO_4^- + 4H^+ + 3e^- \rightarrow MnO_2 + 2H_2O \quad (2.5)$$

$$MnO_4^- + 2H_2O + 3e^- \rightarrow MnO_2 + 4OH^- \quad (2.6)$$

If the cathode has many protons, MnO_4^- reduction will happen faster. The Nernst equation (2.7) predicts that, as a result, the potential at the cathode rises, and the concentration of MnO_4^- at the cathode falls.

$$E = E^0 - \frac{RT}{nF} ln \frac{[MnO_2]}{[MnO_4]} \quad (2.7)$$

(Sudarlin et al., 2020).

In prior research conducted by You (2006), permanganate generated 115.60 mW/m^2 and 0.017 mA/cm^2 as power density and current, which is higher than that produced by hexacyanoferrate and oxygen with only produced 25.62 mW/m^2 and 10.2

Ref. code: 25666422040920FRA

mW/m^2, respectively. Furthermore, a bushing electron acceptor MFC is a permanganate ion obtained at 3986.72 mW/m^2 as a maximum power density with a current at 0.59 mA/cm^2.

However, there are certain flaws in applying permanganate as an electron acceptor. For example, permanganate depletion during power generation needs continual liquid replacements, much like other soluble electron acceptors. Furthermore, because the pH of the solution primarily determines the cathode potential, pH regulation is essential for steady power production, which is only applicable to small-scale power supply. Furthermore, the catalyst does not require for this system (You et al., 2006).

c) Ferricyanide

Ferricyanide is an alternative electron acceptor employed in MFC research. It is because of the unlimited concentration of oxygen. Equation 3.2 showed that the standard redox potential of ferricyanide is lower than oxygen. It has a lot lower overpotential, resulting in a much quicker reaction rate and a much larger power output. A comparison of ferricyanide with a carbon electrode and oxygen with a Pt-carbon cathode shows that due to improved mass transfer efficiency and a more substantial cathode potential, ferricyanide with a carbon electrode generates 50–80% more power (Ucar et al., 2017).

$$Fe(CN)_6^{3-} + e^- \rightarrow Fe(CN)_6^{4-} \qquad (2.8)$$

Although ferricyanide is an efficient electron acceptor for power production, it is acknowledged that there are more realistic long-term solutions than potassium ferricyanide. It is toxic, and chemical regeneration and recycling are challenging. Ferricyanide is a significant cathodic electron acceptor used to prove certain basic principles in the laboratory based on the stability and performance of the system (Logan et al., 2006).

2.3.2 Anodic System

Electron movement from microorganisms, ohmic loss, overpotentials, microbial inoculum, and indirect impacts like electrode cost and cell design all affect

Ref. code: 25666422040920FRA

the power density of MFCs. Bacterial adhesion, electron transport, and substrate oxidation in MFCs are all influenced by the anode materials' composition, shape, and surface characteristics. The ideal anode materials for MFC applications should have good electrode stability in terms of chemical and physical properties, superior conductivity, increased biocompatibility, and low cost (Dumitru & Scott, 2016).

The anode material must be highly conductive and biocompatible. Carbon materials are widespread and appropriate materials for MFC anodes. The high conductivity, stability, solid structure, ample surface area, and ideal surface properties of the carbon material account for this. Bars, foams, slabs, granular carbon, and activated carbon are all examples of carbon that can be used as an anode material (Dumitru & Scott, 2016).

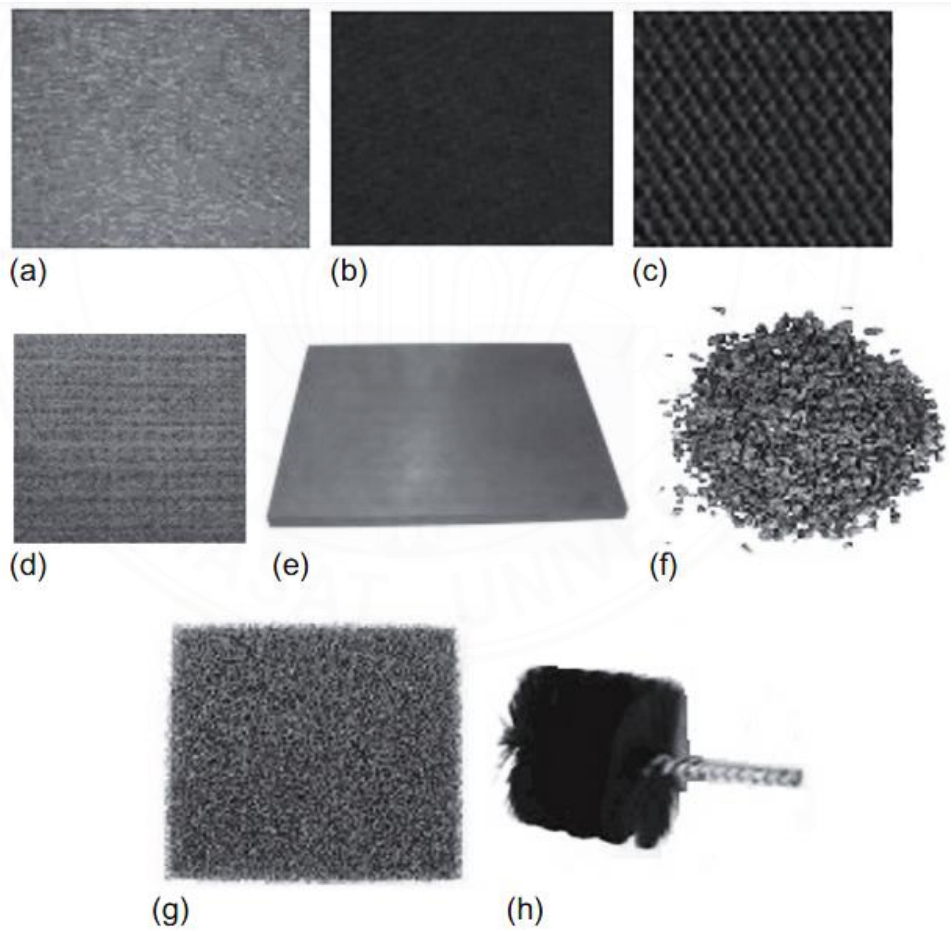

Figure 2.5 (a) carbon paper; (b) carbon cloth; (c) carbon mesh; (d) carbon felt; (e) graphite plate; (f) granular graphite; (g) reticulated verified carbon (RVC); and (h) carbon brush (source: Dumitru & Scott, 2016)

Ref. code: 25666422040920FRA

Research on MFCs made of carbon materials aims to maximize power density per unit of membrane volume or area. Quantitative comparisons between different carbon materials are difficult because other studies, in contrast, have concentrated on the power density of the electrodes' surface area. Published results show that the carbon brush topology offers a higher MFC power density compared to planar configurations like paper, mesh, felt, and sheet (Dumitru & Scott, 2016).

Table 2.2 Various types of carbon anode materials in MFC

Anode materials	Properties	MFC performance	Reference
Carbon paper	Extremely thin, small specific area, simple to connect the wire, expensive, unreliable, and slightly brittle	600 mW/m^2 (bottle-MFC)	Logan et al. (2007)
Carbon cloth	Breathable than carbon paper, thinner, pricey, and greater flexibility	1040 mW/m^2 (cube-shaped MFC)	Logan et al. (2007)
Carbon brush	High surface area and porosities, effecient current collection	2400 mW/m^2 (cube-shaped MFC)	Logan et al. (2007)
Graphite plate	Smooth surface, low specific area, and high cost	3290 mW/m^2	Dewan et al. (2008)
Graphite felt	Thick, large porosity, large resistance, and supportive to bacterial development	386 W/m^3	Aelterman et al. (2008)
Graphite granular	High specific area and low porosities after long-term running	175 W/m^3	Aelterman et al. (2008)

The loss of electrocatalytic activity for microbial processes due to the biofilm clogging pores and reducing efficiency is one of the significant disadvantages of employing carbon material as an MFC anode. These electrodes cannot be employed in large-scale MFCs due to the low specific area, poor durability, brittleness, and high cost of carbon materials (Dumitru & Scott, 2016).

2.4 Modification of Electrode Materials

2.4.1 Modification of Carbon-Based Electrode Materials

CNT and graphene (G) are well-known carbon nanostructures because of their exceptional physicochemical properties, including large surface area, conductivity,

Ref. code: 25666422040920FRA

and mechanical strength. CNTs function flawlessly as anode-modifying components in macro- and micron-sized MFCs. To decrease activation losses and cellular toxicity, surface modification of CNT-based anodes will be necessary. A wide range of bioapplications is now possible thanks to improvements in chemical modification and functionalization methods, which have also boosted the surface activity, processability, and biocompatibility of CNTs (Dumitru & Scott, 2016).

Due to their remarkable features, CNTs have attracted much attention. CNTs are long (up to millimeters), constricted (1100 nm) cylinder structures made of carbon atoms with a cap on each end. CNTs are frequently used as building blocks in complex materials with extraordinary properties after being polished to a high degree of purity. CNT-based structures are used in various applications, including microelectronics, tissue engineering, biosensors, and energy storage materials (Yazdi et al., 2016). This is due to CNT's magnetic characteristics, high surface area to volume (SAV), adsorption capabilities, and biocompatibility.

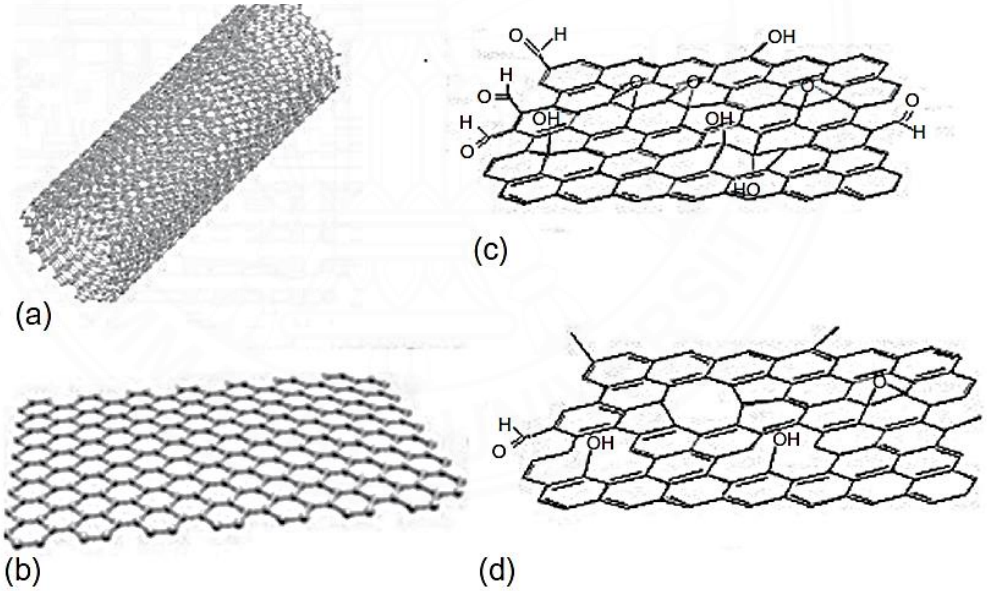

Figure 2.6 Structures of carbon nanostructures, (a) carbon nanotubes (CNTs); (b) graphene (G); (c) graphene oxide (GO); and (d) reduced graphene oxide (rGO).

Researchers working on MFC and nanomaterials can benefit from CNTs, according to numerous studies on CNTs used as electrode materials. Carbon nanotubes significantly improve MFC performance, but CNTs must improve their remarkable biocompatibility with bacterial growth and adhesion. The chemical

Ref. code: 25666422040920FRA

characteristics of the surface can be altered to improve its suitability for practical applications by altering the type of functional groups on the CNT surface (Iftimie & Dumitru, 2019).

Table 2.3 Modification of several anode materials with carbon nanostructures

Carbon nanostructures	Anode	MFC performance	Reference
CNT	Carbon cloth	65 mW/^{2} (up to 250% improvement compared to non-coated CNT)	Tsai et al. (2009)
	Carbon paper	~260 mW/m^2 of maximum power density production	Liang et al. (2011)
	Glassy carbon electrode	The maximum current is 9.7 mA/cm^2, 82 times more than with an anode that has not been changed.	Peng at al. (2010)
Graphene	Stainless steel mesh	18 times greater power density was produced by the unaltered stainless steel mesh anode, which only produced 142 mW/m^2	Zhang et al. (2011)
Graphene oxide	Carbon paper	Power density and current density generated are 34.2 mW/m^2 and 30 A/m^2, respectively	Huang et al. (2011)
Reduced graphene oxide	Carbon cloth	The power density produced is 2.7 W/m^3 compared with 1.7 W/m^3 from the pure CC	Xiao et al. (2012)

2.4.2 Modification of Polymer-Based Electrode Materials

The low electricity generation of the MFC can be effectively overcome by anode modification. The efficiency of electron transfer from microbes can overcome problems with MFC performanceThe efficiency of electron transfer from microorganisms can overcome problems with MFC performance. A high electrical conductivity, increased surface area, porosity, and biocompatibility of the anode material can all be achieved by modification. Additionally, it is essential for MFC commercialization that anode materials are readily available (Dumitru & Scott, 2016).

The type of anode surface being employed affects bacterial adherence and electron transfer. The anode surface can be altered by adding a functional group that is potentially selective against bacteria in order to speed up the mechanism of transferring electrons from bacteria to the anode (Iftimie et al., 2019; Mathew &

Ref. code: 25666422040920FRA

Thomas, 2020). Table 2.4 lists various anodes that have been modified with conducting polymers.

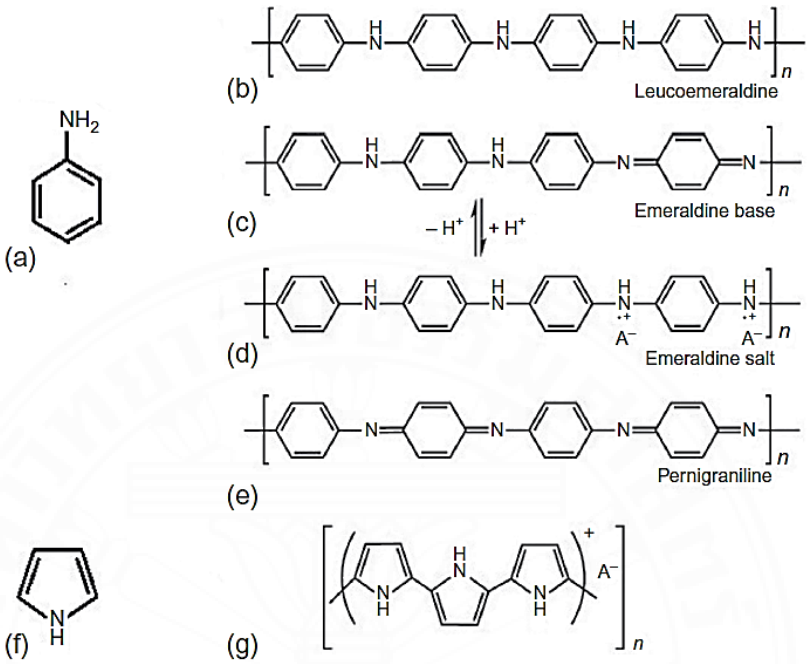

Figure 2.7 Types of conductive polymers: (a) aniline monomer of polyaniline; (b) leucoemeraldine; (c) emeraldinebase; (d) emeraldine salt; (e) pernigraniline; (f) pyrrole monomer, and (g) polypyrrole

Table 2.4 Types of anode modification with conducting polymers

Anode materials	Polymers	Electricity generated	Resources
Carbon felt	PANI	Maximum power density production of carbon felt- modified PANI is 27.4 mW/m^2 commpared with 20.2 mW/m^2 of unmodified carbon felt	Li et al. (2011)
Carbon felt	Poly(aniline-*co*-*o*-aminophenol) (PAOA)	Compared to unmodified carbon felt, carbon felt-PAOA generated power density of 23.8 mW/m^2, which is higher	Li et al. (2011)
Carbon cloth	PANI	Compared to 1.94 W/m^3 of carbon fabric that hasn't been changed, carbon cloth-PANI produces a maximum power density of 5.16 W/m^3	Li et al. (2011)
Carbon fiber	Fibrilar and granular Polypyrrole (PPY)	The power density of modified carbon fiber is 3.4 mW/m^2 while that of untreated carbon fiber is 3.1 mW/m^2	Zou et al. (2010)
Graphite felt	Electrochemically deposited PANI	In comparison to unmodified graphite felt, PANI's maximum power density	Wang et al. (2014)

Ref. code: 25666422040920FRA

Anode materials	Polymers	Electricity generated	Resources
RVC	PPY	production is 4 W/m^3, which is higher RVC-PPY modified produces a maximum power density of 1.4 mW/cm^3 compared to 0.42 mW/cm^3 for original RVC	Balint et al. (2014)

2.5 Polyaniline (PANI)

PANI is a conducting polymer with good environmental stability, relatively high electrical conductivity, high surface-to-volume ratio, inexpensive, and easy to synthesize in the laboratory. These properties make PANI a conducting polymer that is widely used to modify electrodes (Ashokkumar et al., 2020). In addition, their nanocomposites are ideal coating materials for MFC electrodes, resulting in significant power increases. PANI is a redox-active catalyst and increases capacitance values in energy devices (Mathew & Thomas, 2020). Table 2.5 shows the FTIR spectrums of PANI that can be used to identify PANI structure on electrode modification (Shih et al., 2017; Yin et al., 2019; Zhang et al., 2021). One kind of polymer that has received much attention in electrochemical applications is PANI. Its oxidation and protonation determine its exceptional chemical and physical characteristics. Despite having a nanostructure, PANI is a polymer that is simple to make. Using PANI to modify the anode proved effective in improving the performance of the MFC system. The PANI is used to modify a variety of anodes in MFCs, including carbon and platinized carbon cloth coated with PANI, glass carbon nanostructured with PANI, electrochemically deposited PANI on graphite fiber, carbon cloth coated with H_2SO_4-doped PANI, and indium tin oxide conductive glass modified using PANI-NN (Dumitru & Scott, 2016).

PANI can be used as the primary nanomaterial for electrode coating. According to Matthew and Thomas (2020), the conductivity qualities of PANI will enhance the electrode's surface area and decrease the resistance of extracellular microbial electrical transmission to the electrode surface, enhancing the production of MFC electricity. TiO_2-20PANI/CP and TiO_2-NS/CP, two types of carbon paper with TiO_2 modifications, were used as the anode materials in Yin et al.'s (2019) investigation on the performance of MFCs. According to the research, the most

Ref. code: 25666422040920FRA

excellent power density for MFC using TiO_2-20PANI/CP is 813 mW/m^2. According to this finding, with the TiO_2-NS/CP anode, MFC increased by 63.6% (without adding PANI). This is owing to the synergistic effect of vertically aligned TiO_2-NS and PANI, which considerably reduces the charge transfer resistance at the anode contact. This highlights the ability of polymer compounds to modify anodes to give bacteria good environmental stability.

Table 2.5 FTIR characterization of PANI

FTIR spectra	Functional group
1590, 1508 and 1308 cm^{-1}	Aniline's quinoid and benzenoid rings and nitro aniline's ring stretching vibrations
1595 and 1560 cm^{-1}	Aniline and nitro-aniline ring segments undergo quinoid stretching
1385 cm^{-1}	Stretching of $C=N^+$ next to the quinoid
1310 cm^{-1}	The alternative units of quinoid benzenoid quinoid rings have a structure of C–N stretching vibration
1304 and 1210 cm^{-1}	N–H bending and the C–C (or C–N) stretching modes' symmetric component
1510 and 1346 cm^{-1}	Stretching modes of asymmetric and symmetric of the nitro group of o-nitro aniline

Ref. code: 25666422040920FRA

CHAPTER 3
METHODOLOGY

This section describes in detail the materials used in the research, the components and dimensions of the MFC reactor used, the material preparation methods and research procedures, as well as the chemical analysis method and data analysis from the operation of the MFC reactor. This study was conducted based on several stages, which are listed below:

3.1 Preparation of Polyaniline (PANI)

PANI can be created through the chemical polymerization of aniline hydrochloride when ammonium peroxydisulphate is used as an oxidizing agent. Aniline hydrochloride and ammonium peroxydisulphate dissolved separately in one molar of hydrochloric acid had a molar ratio of 1:1.25 in the presence of an aqueous acid solution. The solution was continuously stirred for four hours at 0^{o}C and kept at room temperature for polymerization for 24 hours. The polymerized salt was filtered and washed with double-distilled water and one molar of HCl to eliminate the contaminants. PANI salt was dried in a hot air oven at 60^{o}C in the last step (Mathew & Thomas, 2020).

3.2 Modification of Electrode Materials

3.2.1 Preparation of Aniline Monomer Solution

The aniline monomer solution was prepared in an acidic medium by dissolving 9.3 grams of aniline hydrochloride (99%) from Thermo Scientific in 54.2 mL H_2SO_4. Then the solution was added with deionized water until it reached a total volume of 1 liter. The aniline solution is stirred slowly until it is homogeneous.

3.2.2 Electropolymerization on Graphite Carbon Electrodes (GCE)

The manufacture of PANI-modified GCE was carried out by the EPD method. The EPD is carried out using a DC power supply. This system is a system with two electrodes. The GCE is connected to the positive charge, and the platinum electrode is

Ref. code: 25666422040920FRA

connected to the negatively charged part of the system. The electric current of 2.5 Volt flows through the power supply for 10 minutes. The aniline monomer solution is the electrolyte solution in this system. Aniline monomer will flow over the surface of the graphite carbon rod to form a PANI layer (polymer film) and the modification result identified as GCE-PANI. After the coating process is done, wash the GCE-PANI with deionized water and keep it until it is dry before use.

3.2.3 Eleectropolymerization on Activated Carbon Cloth (ACC)

The PANI polymerization process on the activated carbon cloth surface used electrophoretic deposition with a DC power supply. The activated carbon cloth electrode is connected to the positive charge, and the platinum electrode is connected to the negatively charged part of the system. The potential of 2.5 Volt flows through the power supply for 10 minutes. The aniline monomer solution is the electrolyte solution in this system. The aniline monomer will flow over the surface of the activated carbon cloth to form a PANI film. The modification result is identified as ACC-PANI. After the coating process is done, wash the ACC-PANI with deionized water and keep it until it is dry before use.

3.2.4 Eleectropolymerization on Activated Carbon Cloth-Carbon Tape (ACC-CT)

The PANI polymerization process on the ACC-CT surface used the same reaction as the previous two modifications on GCE and ACC. Before the coating reaction started, carbon tape (CT) was first put in the middle of ACC on both sides. The CT on the ACC surface was used to evaluate the different conductivity between the ACC and ACC-CT when it was modified with PANI. The ACC-CT is connected to the positive charge, and the platinum electrode is connected to the negatively charged part of the EPD system. The potential of 2.5 Volt flows through the power supply for 10 minutes during the reaction. The electrolyte solution in this system is aniline monomer. The aniline monomer will flow over the surface of the ACC-CT to form a PANI film identified as ACC-CT/PANI. After the coating process is done, the ACC-CT/PANI was washed with deionized water, and dried before use. The schematic diagram of electrophoretic deposition is shown in Figure 3.1.

Ref. code: 25666422040920FRA

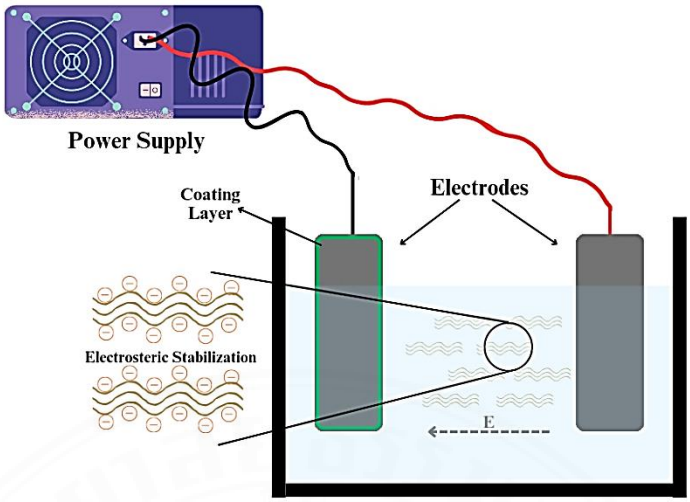

Figure 3.1 Illustration of EPD system

3.3 Characterization of Modified Electrodes

3.3.1 FTIR Characterization

FTIR characterization will be used to identify the structure of polyaniline and polypyrrole on modified graphite carbon electrodes. The area of IR spectroscopy radiation ranges from the wave number 12800-10 cm^{-1}, or the wavelength 0.78-1000 m, while the area commonly used for practical purposes is in the wave number between 4000-400 cm^{-1}. The instrument used was FTIR (Nicolet iS50, Thermo Scientific, USA) with Attenuated Total Reflectance (ATR) testing mode. FTIR spectra for PANI refer to Table 2.5.

3.3.2 FESEM Characterization

GCE, GCE-PANI, ACC, and ACC-PANI surfaces were investigated using Field Emission Scanning Electron Microscopy (JEOL JSM7800F, Japan). Measurements were tested with a magnification of 100 – 10000x at the surface area of the samples. The morphology of the surface shape of carbon graphite and carbon cloth before being modified with PANI coating was compared to that which had been modified based on the photo of the FESEM test results.

3.3.3 BET (Brunauer, Emmett, and Teller) Characterization

The instrument used was Surface Area Analyzer (3Flex, Micromeritics, USA). he BET analysis determines the surface area of the graphite carbon electrode and the

Ref. code: 25666422040920FRA

pore distribution under conditions before and after being modified with a conductive polymer coating. In this study, the BET test conditions were carried out by setting the nitrogen adsorption temperature at 77 K, with a saturated vapor pressure of 102.95 kPa. The samples were pretreated and heated to 423 K (150 ^{o}C) for 6 hours while nitrogen gas flowed through the chamber. This test will also compare the results of surface area and pore distribution between GCE-PANI and ACC-PANI.

$$\frac{1}{W[(^{Po}/_{P})]-1} = \frac{1}{Wm\,C} + \frac{C-1}{Wm\,C}\left(\frac{P}{Po}\right) \quad (3.1)$$

where W is the mass of the adsorbed gas, W_m is the mass of the gas adsorbed monolayer, the pressure of the adsorbed gas is stated by P, while P_0 is the pressure saturated vapor of the adsorbate at room temperature, and C is the BET constant. The surface area of SBET (m^2g^{-1}) is calculated from the value of W_m with the equation:

$$S = \frac{Wm \times N \times A}{M} \quad (3.2)$$

where the N value is 6.023 × 1023 molecules/mol which is the number of Avogadro constant, A is the surface area of the adsorbed molecule (A of N_2 gas is 16.2×10^{-20} m^2), and the adsorbate's molecular weight stated by M (the molecular weight of N_2 is 28.0134 g/mole).

The gas adsorption method for determining pore size and pore distribution is based on the Kelvin equation which relates pressure to pore size, as follows:

$$\ln\frac{P}{Po} = -\frac{2\gamma V}{rRT}cos\theta \quad (3.3)$$

where P is the adsorbed liquid's pressure at the pore radius (r), V and γ are the molar volume of the liquid and surface tension, and θ is the contact angle of the liquid with the pore walls. Total pore volume is the volume of gas adsorbed at its saturation pressure, assuming that there is no surface outside the pore walls. Therefore, the average radius can calculate using a cylindrical geometry equation starting from the ratio of the total pore volume and the surface area of BET.

$$\frac{r}{2} = \frac{Vp}{S} \quad (3.4)$$

Ref. code: 25666422040920FRA

with r is the average radius and V_p is the total pore volume.

3.3.4 Cyclic Voltametry Analysis

The CV is used to study specific capacitance between the modified and unmodified electrodes. CV was measured by an autolab PGSTAT 302N potentiostat/galvanostat (Metrohm) in an electrochemical cell. For electrochemical activities, the electrochemical cell contained samples of GCE, GCE-PANI, ACC, and ACC-PANI as working electrodes, a platinum plate electrode as a counter electrode, and an Ag/AgCl as the reference electrode. Sodium chloride (NaCl) 0.5 M was applied as an electrolyte for the system. The potential range was swept between −0.8 to 1.0 V for five cycles using the scan rates of 25, 50, 100, and 200 mV s^{-1} (for GCE and GCE-PANI) and the scan rates 5, 10, 15, and 20 mV s^{-1} (for ACC and ACC-PANI). Furthermore, the electrode materials were rinsed with deionized water several times and dried at room temperature. The CV measurement was calculated to analyze the specific capacitance following Equation (3.5).

$$C_P = \frac{A}{2 \times m \times k\ (V_2 - V_1)} \tag{3.5}$$

Where *A* refers to the total area of the CV graph, C_p is the specific capacitance, *m* is for the mass of the electrode, *k* is the scan rate applied to the system, and $(V_2 - V_1)$ stands to the range of potential window.

3.4 Wastewater Preparation

3.4.1 The UASB Sludge Sampling

This research used the microorganisms from the sludge sample from the Up-flow Anaerobic Sludge Blanket (UASB) reactor wastewater treatment plant. The sludge was sampled at the UASB tank and aerobic tank's effluent to minimize the contamination content in the sample. The UASB sludge was sampled from the Pathum Thani Brewery Co., Ltd. located on Soi Chai Uea, Bang Khu Wat, Mueang Pathum Thani District, Pathum Thani, Thailand.

The sludge sample is stored in a plastic container to avoid falling and breaking with a rubber gasket sealed (to prevent leaking). The container saves in an enormous rigid plastic container with the outer container filled with PE foam to minimize the

Ref. code: 25666422040920FRA

spread of contaminants. Figure 3.2 illustrates of the sampling procedure from the company to the SIIT's biosafety laboratory.

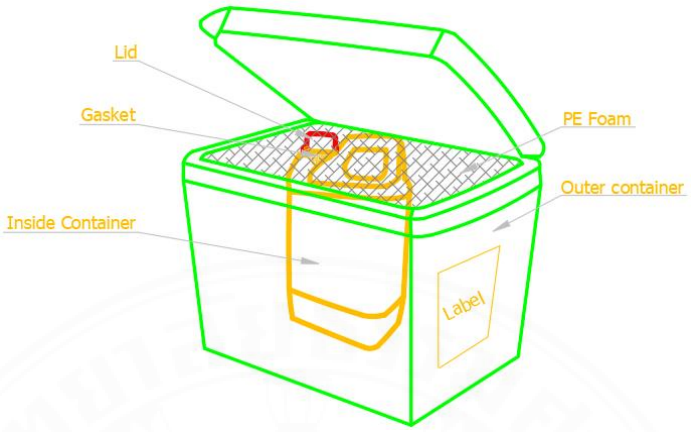

Figure 3.2 The illustration of the container to bring the UASB sludge

3.4.2 Preparation of Trace Nutrient

The trace nutrient solution was prepared following Virdis et al. (2011). It is consisted of: 1.5 grams of $FeCl_3.6H_2O$, 0.15 grams of H_3BO_3, 0.03 grams of $CuSO_4.5H_2O$, 0.18 grams of KI, 0.12 grams of $MnCl_2.4H_2O$, 0.06 grams of $Na_2MoO_4.2H_2O$, 0.12 grams of $ZnSO_4.7H_2O$, 0.15 grams of $CoCl_2.6H_2O$, and 10 grams of EDTA (Ethylenediamine tetra-acetic acid) from Loba Chemie Pvt. Ltd. with purity of all chemicals were 99%.

3.4.3 Synthesis of Artificial Wastewater

Stock media based on Lu et al. (2006) for artificial wastewater in this study contained 6 grams of Na_2HPO_4, 3 grams of KH_2PO_4, 0.5 grams of NaCl, 0.1 grams of $MgSO_4.7H_2O$, and 0.015 grams of $CaCl_2.7H_2O$. The synthetic wastewater prepared had a COD of 1000 mg/L, which was obtained by adding 1.28 grams of CH_3COONa to 1 liter of stock media solution. The synthetic wastewater used in the MFC reactor consists of a mixture of 1000 mg/L COD stock media solution and trace nutrient solution with a ratio of 70:30. Sludge samples from a brewery wastewater treatment plant in Thailand were used to fill 20% of the total capacity of the MFC anode reactor to grow microbial cultures during the acclimatization process.

Ref. code: 25666422040920FRA

3.5 Configuration of MFC

Two double-chamber MFCs with cathode and anode are made using 10 mm thick acrylic plates, with the dimensions of each chamber (50 × 50 × 100) mm. Each chamber of the reactor has a capacity of 250 mL. CEM separated the two chambers of each MFC reactor with a surface area of 264 cm^2 (CMI-7000S, Membrane International, USA). The design of the reactor is shown in Figure 3.3.

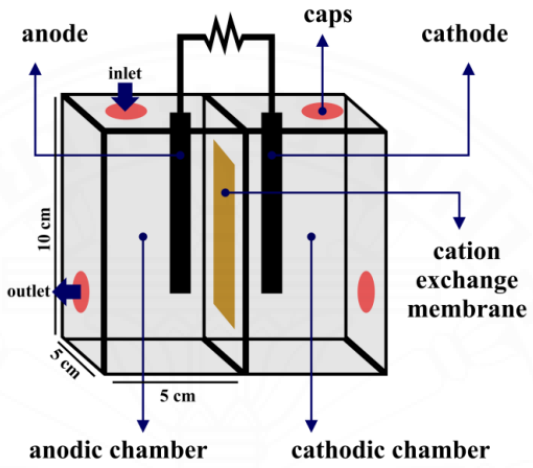

Figure 3.3 MFC reactor design

The electrodes used in this study were GCE, GCE-PANI, ACC, and ACC-PANI as an anode. The cathode were GCE and ACC. The GCE is a graphite rod with a length of 100 mm and a diameter of 10 mm. In contrast, the shape of ACC is rectangular with (50 × 100) mm dimensions. Before use, the GCE was cleaned and activated in acidic (1 M HCl) and alkaline (1 M NaOH) solutions for 24 hours, respectively. After that, the electrodes were stored in distilled water until used to remove metals and other contaminants (Sejati & Sudarlin, 2020).

Furthermore, the pre-treatment for the ACC was sonicated for 15 minutes each using acetone, 1 M H_2SO_4, ethanol, and deionized water. External resistors with 500-ohm resistance and copper wires are used to connect the external circuit components of the reactor with data loggers connected to computer devices. The MFC reactor is shown in Figure 3.4.

Ref. code: 25666422040920FRA

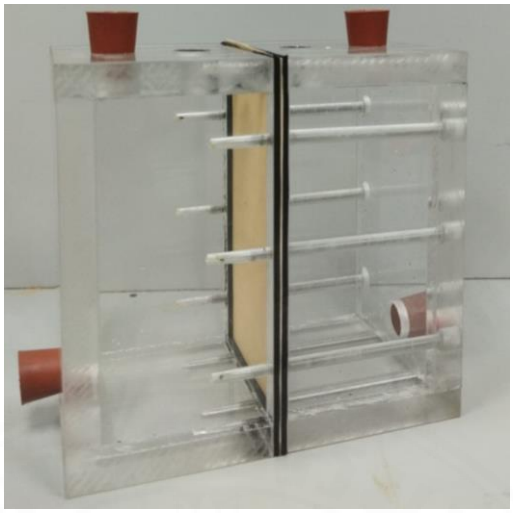

Figure 3.4 The MFC reactor

3.6 Operation of MFC

Two MFC reactors operate at room temperature of 20−25 ^{o}C. The first system is MFC with a GCE-based anode, and the second is with an ACC-based anode. The external resistance of both MFCs was set at 500 ohms. The cathodic chamber is filled with an electrolyte solution as an electron acceptor. The first system filled with water and oxygen flow as an electron acceptor, while the second system used $K_3[Fe(CN)_6]$. The anode chamber is filled with synthetic wastewater with the composition described in section 3.4. The start-up stage was successful after the MFC reached a steady state when the current stabilized and contaminant removal was obtained. The electricity production from the MFC reactor was monitored every day. The COD content was evaluated whenever there was a significant decrease in electricity production (end of the MFC's operating cycle). When the current generated from the MFC system has already dropped and the result of the COD removal test showing the rest of the COD content in an anodic chamber lower than 200 mg/L (about 80% removed), the system is refreshed by changing the wastewater in an anodic chamber with the new wastewater 1,000 mg/L COD to start the second cycle of MFC. Every system of MFC was operated within two cycles in this experiment. The working schemes of the MFC reactor are shown in Figure 3.5 and Figure 3.6. The MFCs system operated in this study consists of the following system,

a. MFC with GCE-anode and oxygen electron acceptor.
b. MFC with GCE-PANI-anode and oxygen electron acceptor.

Ref. code: 25666422040920FRA

c. MFC with GCE-anode and $K_3[Fe(CN)_6]$ electron acceptor.
d. MFC with GCE-PANI-anode and $K_3[Fe(CN)_6]$ electron acceptor.
e. MFC with ACC-anode and oxygen electron acceptor.
f. MFC with ACC-PANI-anode and oxygen electron acceptor.
g. MFC with ACC-anode and $K_3[Fe(CN)_6]$ electron acceptor.
h. MFC with ACC-PANI-anode and $K_3[Fe(CN)_6]$ electron acceptor.
i. MFC with ACC-CT-anode and oxygen electron acceptor
j. MFC with ACC-CT/PANI-anode and oxygen electron acceptor

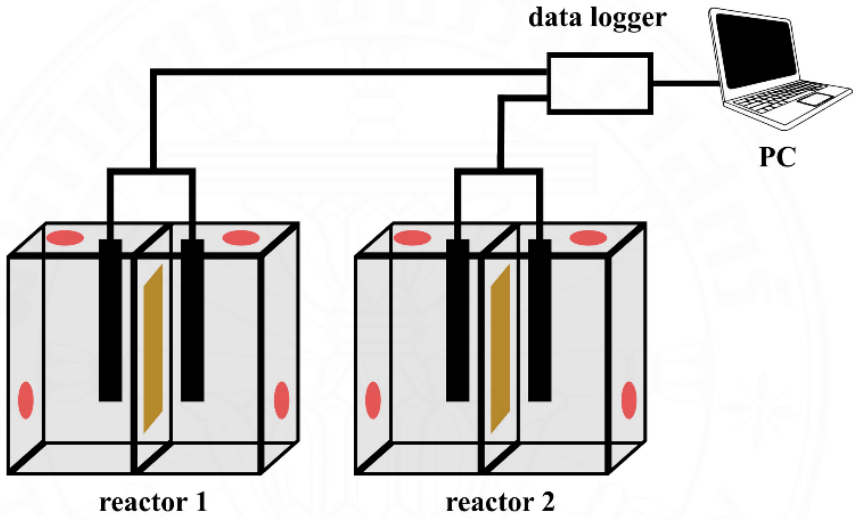

Figure 3.5 Diagram of the MFC with $K_3[Fe(CN)_6]$ as electron acceptor

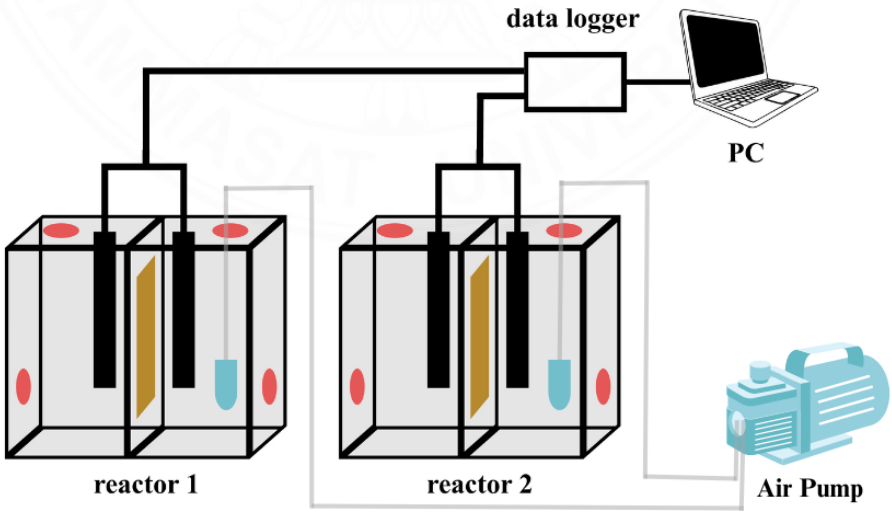

Figure 3.6 Diagram of the MFC with oxygen as electron acceptor

Ref. code: 25666422040920FRA

3.7 Chemical Oxygen Demand (COD) Analysis

A strong chemical oxidant is added to a sample and incubated with it for a predetermined time and at a predetermined temperature (often 2 hours at 150°C) in a laboratory experiment to determine COD. When combined with sulphuric acid that has been heated up, potassium dichromate is the most often employed oxidant. The COD analysis follows the standard method (SNI 6989.73−2009) with the steps are followed,

3.7.1 Preparation of Digestion Solution $K_2Cr_2O_7$ 0.1 N

As many as 4.803 grams of $K_2Cr_2O_7$ were heated at 150 ^oC for two hours and dissolved in 500 mL of deionized water. then 167 ml of H_2SO_4 and 33.3 grams of $HgSO_4$ were added to the $K_2Cr_2O_7$ solution. After the mixed solution becomes homogeneous, deionized water is added to the solution until it reaches a total volume of 1 liter.

3.7.2 Preparation of Sulphuric Acid

The Ag_2SO_4 weighed as much as 10.12 grams and dissolved in 1 liter of H_2SO_4. Stir the solution slowly until all the Ag_2SO_4 solids are entirely dissolved. This dissolving process can take up to a day.

3.7.3 Preparation of Ferroine Indicator

The 1.485 grams of 1,10-phenanthroline monohydrate was dissolved in 100 mL deionized water and added with 0.695 grams of $FeSO_4.7H_2O$. The mixture is stirred until completely dissolved and homogeneous.

3.7.4 Preparation of Ferrous Ammonium Sulfate (FAS) 0.05 N

Ferrous ammonium sulfate (FAS) solution was prepared by dissolving 19.6 grams of $Fe(NH_4)_2.(SO_4)_2.6H_2O$ in 300 mL of deionized water. After all the solids were completely dissolved, 20 mL of H_2SO_4 was added to the solution, and deionized water was added to a total volume of 1 liter. After the FAS solution has been prepared, the FAS solution is standardized before being used for the titration process in the COD test. 5 mL of $K_2Cr_2O_7$ digestion solution is added with 10 mL deionized

Ref. code: 25666422040920FRA

water and two drops of ferroin indicator. The mixtures of digestion solution mixed with water were titrated using FAS solution. FAS solution concentration can be calculated using the following equation,

$$N_{FAS} = \frac{(V_K \times N_K)}{V_{FAS}} \quad (3.6)$$

where N_{FAS} is the concentration of FAS solution; V_{FAS} is the volume of FAS solution used to titrate the mixture of digestion solution and water; V_K is the volume of digestion solution; and N_k is the concentration of digestion solution.

3.7.5 COD Test and Calculation

The 5 mL of wastewater samples were prepared in a test tube. Wastewater samples were added with 3 mL of digestion solution and 7 mL of H_2SO_4 solution. This solution mixture was heated for 2 hours at 150 ^oC. After that, the sample solution mixture was cooled to room temperature and transferred into the Erlenmeyer. The two drops of ferroin indicator were added to the sample mixture and titrated using a standardized FAS solution. Determination of COD levels is calculated using the following equation,

$$COD = \frac{(V_b - V_a) \times N_{FAS} \times p \times 8000}{V_s} \quad (3.7)$$

where V_b is the titration volume of blank (water); V_a is the titration volume of the wastewater sample; N_{FAS} is the standardized FAS solution's concentration, p is the dilution, and 8000 is the oxygen equivalent value.

3.7.6 Wastewater Treatment Efficiencies

The treatment efficiency (R%) can be determined based on the analysis and comparison of the COD level of the wastewater before and after being treated with the MFC system. Calculation of efficiency and removal rate of COD level in wastewater treatment is measured using the following Equations (3.8),

$$R\% = \frac{C_0 - C_1}{C_0} \times 100 \quad (3.8)$$

Ref. code: 25666422040920FRA

the C_0 and C_1 are the COD levels before and after treatment.

3.8 Sludge and Wastewater Control During and After Experiments

The UASB sludge inoculates in an MFC reactor with synthesis wastewater. The work area is the biosafety lab, restricted to authorized personnel. All experiments are performed to minimize the risk of producing splashes and aerosols following the biosafety regulation at Thammasat University. Before and after the experiment, the working surface area was cleaned and disinfected with a 70% alcohol solution to decontaminate most microorganisms in the sludge. All items and equipment that have come in contact with sludge or wastewater of the MFCs system will be decontaminated after use with 70% alcohol solution, limiting the spread of contamination beyond the work area and facility. Before disposal of wastewater or sludge, it will be treated in autoclaves at 121 ^{o}C for a minimum of 15 minutes to inactivate all microorganisms, thanks to the effectiveness of exposure to high-pressure saturated steam.

3.9 Energy generation Analysis

3.9.1 Potential (V)

The potential or voltage in this study was obtained based on the measurement results using a data logger per minute of reaction. The voltage measurement every minute is intended to monitor the reaction process while the MFC is running.

3.9.2 Current (I)

The current is calculated using Ohm's law equation in Equation (3.9), where V is the measured voltage in section 3.10.1, and R is the external resistance used in the study.

$$I = \frac{V}{R} \tag{3.9}$$

3.9.3 Current Density (I_d) and Power Density (P_d)

The current density (I_d) and power density (P_d) are calculated based on the surface area of the electrode used using Equation (3.10) and Equation (3.11),

Ref. code: 25666422040920FRA

respectively. V is the rated voltage of the system, R refers to the external resistor, and A is the surface area of the electrodes.

$$I_d = \frac{V}{A \times R} \tag{3.10}$$

$$P_d = \frac{V^2}{A \times R} \tag{3.11}$$

3.9.4 Normalized Energy Recovery (NER) and Current Efficiency (CE)

Equations (3.12) and (3.13) were used to determine the normalized energy recovery based on the volume of the treated wastewater in an anode chamber (NER_V) and the amount of COD removed in an anode chamber (NER_{COD}), respectively. P stands for power, T for treatment time, V_a for anodic chamber volume, and ΔCOD stands for the volume of COD eliminated in an anode chamber.

$$NER_V = \frac{P \times T}{V_a} \tag{3.12}$$

$$NER_{COD} = \frac{P \times T}{\Delta COD} \tag{3.13}$$

The current efficiency (CE) indicating the percentage of the electrolytic reaction in the MFC reactor is shown by Equation (3.14). In the equation, P stands for power, T for treatment time, V_a for anodic chamber volume, ΔCOD stands for the volume of COD eliminated in an anode chamber, M is the molecular weight of a displaced element, i is a current in Amperes, t is the reaction time in seconds, N is oxidation state, and F refers to Faraday's constant (96,487 Coulombs).

$$CE = \frac{(M \times i \times t)}{(N \times F)} \times 100\% \tag{3.14}$$

3.10 Salt Analysis

The salt analysis is done by first making a standard metal solution. After that, the salt sample formed on the surface of the MFC reactor was taken and dissolved in deionized water with a concentration of 1 ppm of salt sample solution. The prepared salt sample solution was analyzed using Inductively Coupled Plasma-Optical Emission Spectrometer (ICP-OES Perkin Elmer, Avio 200) to detect the metals oxidized during the process.

Ref. code: 25666422040920FRA

3.11 Flow Chart of Experiments

The flow chart in this experiments is shown in Figure 3.7.

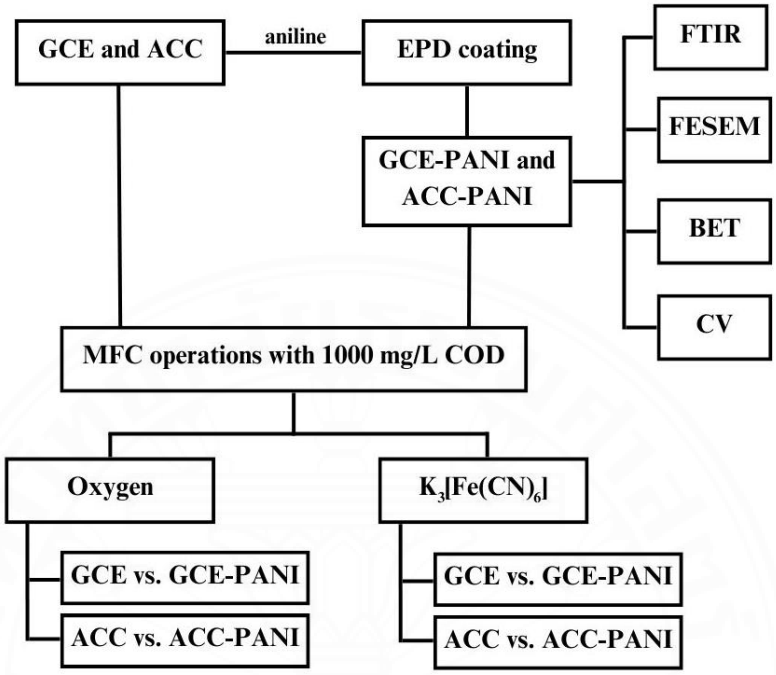

Figure 3.7 Flow chart of experiments

Ref. code: 25666422040920FRA

CHAPTER 4
RESULTS AND DISCUSSION

4.1 Synthesis of PANI

PANI was synthesized as a standard to determine the structure of PANI on the modified GCE and ACC surfaces to prove that the coating process during modification succeeded. The PANI structure was checked with FTIR to compare pure graphite and PANI-coated graphite electrodes. Figure 4.1 shows the FTIR spectra of PANI synthesized. The peaks at 1557 cm^{-1} demonstrated the existence of quinoid rings (Q) caused by the N=Q=N stretching vibration. The 1479 and 1400 cm^{-1} peaks were due to PANI's N−B−N stretching mode (B means benzenoid ring). The peak near 1303 cm^{-1} belonged to the C−N−C stretching vibration, while the peak at 1244 cm^{-1} was attributed to the aromatic amine's C−N stretching (Zhang et al., 2021). The peak at 1140 cm^{-1} refers to the C−H in-plane bending, and the peaks around 880, 807, and 705 cm^{-1} were related to the C−H substituted benzene out-of-plane bending. The S=O in-plane bending appears at 591 cm^{-1} (Shih et al., 2017). The peak at 508 cm^{-1} was related to the out-of-plane bending vibrations of C−H and C−C in benzenoid units (Zhang et al., 2021). The quinoid ring and benzenoid ring on the PANI structure are illustrated in Figure 4.2.

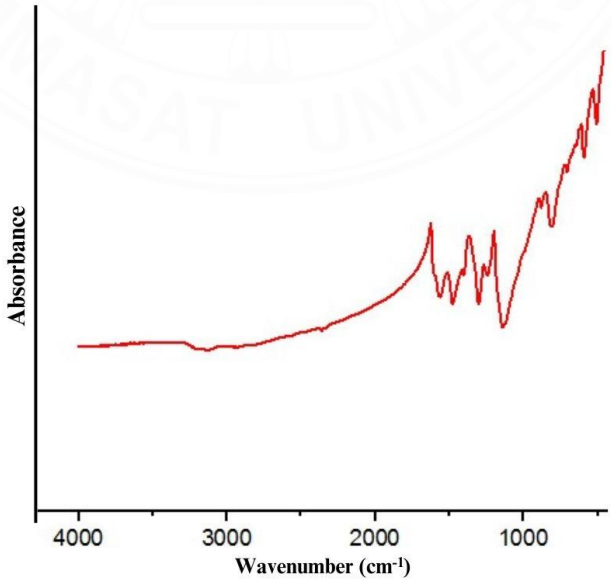

Figure 4.1 FTIR spectra of PANI structure

Ref. code: 25666422040920FRA

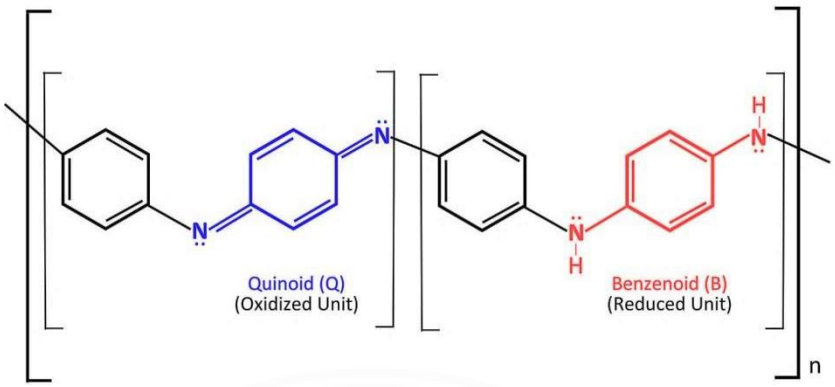

Figure 4.2 Structure of PANI

4.2 Electropolymerization of PANI

The PANI was coated on the surface of GCE and ACC with an EPD technique electrochemically. The polymerization reaction of aniline to become PANI is called the electrochemical particle coagulation mechanism. Based on the reaction mechanism illustrated in Figure 4.3, electrolyte concentration will increase on the cathode side. When a voltage of 2.5 volts is applied through the power supply to the system, the concentration of aniline monomer will increase around the cathode area. An increase in the concentration of aniline monomer will form a thin film layer on the surface of the electrode, which becomes more and more concentrated to form a polymer form, namely polyaniline, which is the result of this modification in this study called a GCE-PANI and ACC-PANI. This explanation aligns with the reaction illustrated by Corni et al. (2008) that the zeta potential dropping near the electrode is essential for producing the deposition. It happened because the electrolyte concentration increases close to the electrode when an electric field is present. Then, the locally concentrated electrolyte causes the suspension to flocculate, producing the thin polymer layer on the cathode surface.

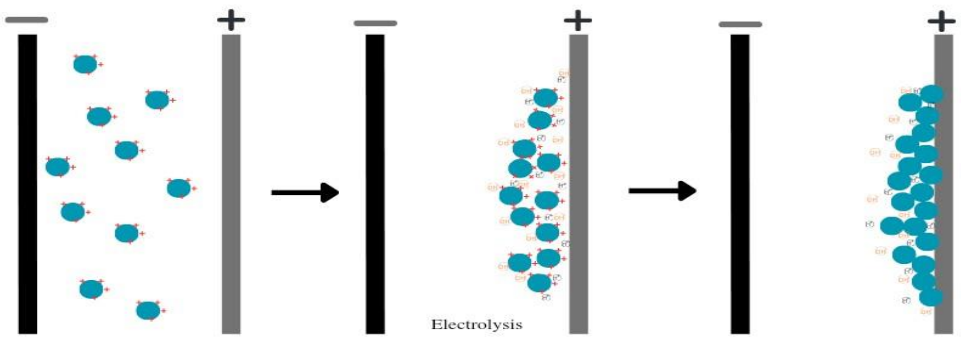

Figure 4.3 Electrochemical particle coagulation on EPD coating process

Ref. code: 25666422040920FRA

4.3 Modification of GCE

The PANI layer on the graphite carbon electrode's surface organoleptically looks dark green. The color difference indicates the presence of a PANI layer formed on the graphite surface. The result of GCE-PANI is shown in Figure 4.4.

Figure 4.4 GCE-PANI

4.3.1 FTIR Analysis of GCE-PANI

FTIR examined the structure of unmodified GCE and GCE-PANI. A comparison between the three FTIR spectra of PANI, GCE, and GCE-PANI is shown in Figure 4.5. It can be seen from the figure that the graphite carbon only shows two spectra in the wave number range of 3400 and 1500 cm^{-1}. As for the analysis results of the PANI-coated graphite carbon electrode, it shows an appearance of the PANI spectra in the wavenumber region between 500 - 1600 cm^{-1}. The results of the analysis and comparison of the three FTIRs are shown in Table 4.1 (Shih et al., 2017; Yin et al., 2019; Zhang et al., 2021).

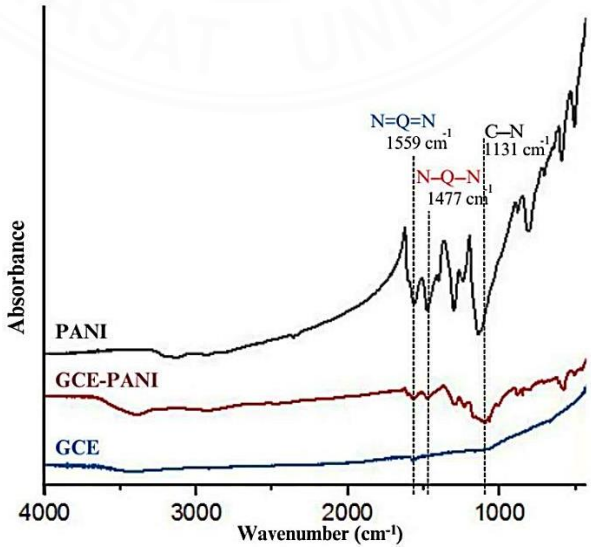

Figure 4.5 Comparison of FTIR between unmodified GCE and GCE-PANI

Ref. code: 25666422040920FRA

Table 4.1 The FTIR analysis and comparison between GCE and GCE-PANI

FTIR of GCE	FTIR of PANI	FTIR of PANI-GCE	Assignment
Wavenumber (cm^{-1})	Wavenumber (cm^{-1})	Wavenumber (cm^{-1})	
3442		3394	C−C stretching
		2921	C−H stretching
	1577	1559	N=Q=N stretching in quinoid rings
	1479	1477	N−B−N stretching in benzenoid rings
	1303		C−N−C stretching vibration
	1244	1289	C−N stretching
	1140	1171	C−H in-plane bending
	880	884	C−H substituted benzene out-plane bending
	807	850	
	705		
	591	582	S=O in-plane bending
	508	510	C−H and C−C in benzenoid units or amine deformation

4.3.2 SEM Analysis of GCE-PANI

The surface morphology of the PANI film on graphite carbon electrode is shown in Figure 4.6 before and after being coated with a PANI layer. It can be seen that the GCE surface in Figure 4.6(a) has an irregular structure. PANI electrodeposition on the GCE surface showed excellent results. Figure 4.6(b) shows that a PANI layer has covered the GCE surface. The PANI layer has a porous structure. In addition, there appears to be an increase in surface coverage by polymeric materials due to an increase in the deposition rate (Mello et al., 2018). The morphology of PANI, which partially forms a micron-sized pore structure, is beneficial for the growth of microorganisms inside the electrode (Zhang et al., 2017; Yin et al., 2019). With this porosity, a film should have quicker charging (doping) and discharging (dedoping) current responses (Kaneda et al., 2020).

Ref. code: 25666422040920FRA

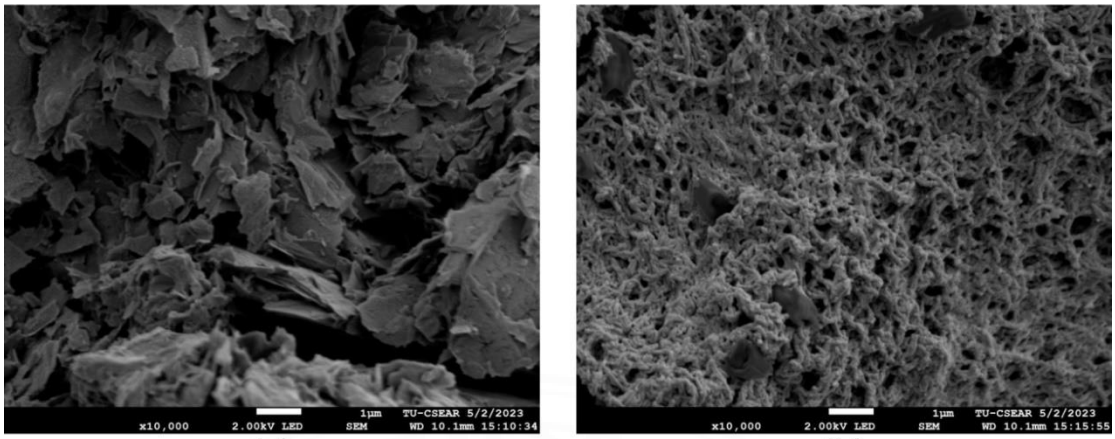

Figure 4.6 FESEM micrographs of (a) GCE; and (b) GCE-PANI

4.3.3 BET Analysis of GCE-PANI

The BET test was carried out to analyze the condition of the surface of the graphite electrode before and after being modified with polyaniline coating. The results of N_2 adsorption and desorption studies are shown in Figure 4.7 by comparing GCE and GCE-PANI. Figure 4.7 shows the shape of the type IV isotherm, which indicates that a porous structure with a mesoporous type is found on the surface of the GCE and GCE-PANI electrodes. The first part of the curve, which coincides, is also associated with monolayer–multilayer adsorption, which supports the mesoporous structure of the sample (Kajama et al., 2015). Details of the surface characteristics of the GCE and GCE-PANI electrodes are shown in Table 2.

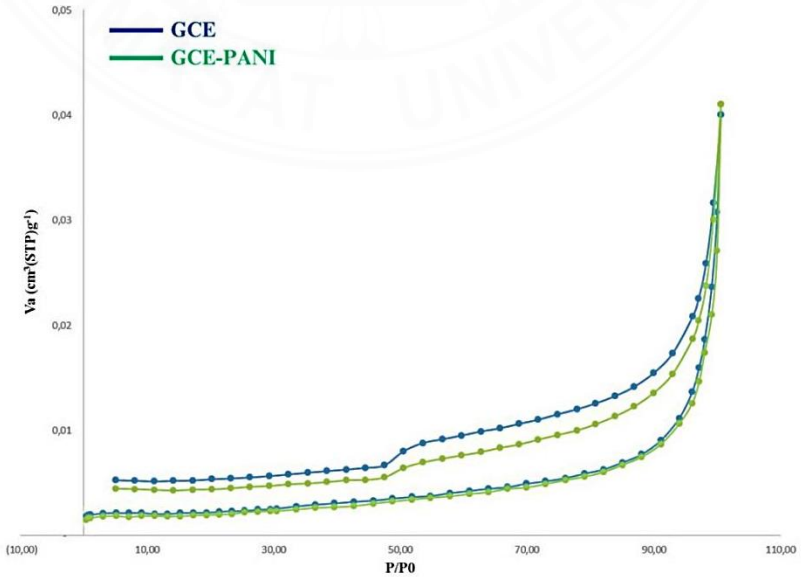

Figure 4.7 N_2 adsorption/desorption curve of GCE anf GCE-PANI

Ref. code: 25666422040920FRA

Table 4.2 Surface characteristics of GCE and GCE-PANI

Electrodes	BET Surface Area (m^2/g)	Pore Volume (cm^3/g)	Average Pore Size (Å)	Average Particle Size (Å)
GCE	0.20	4.79×10^{-4}	94.56	296,115.01
GCE-PANI	0.17	4.40×10^{-4}	101.18	344,790.93

4.3.4 Electrochemical Analysis of GCE-PANI

Electrochemical characteristics were analyzed by CV testing, shown in Figure 4.8. Measurements with variations of four scan rates (25 mVs^{-1}, 50 mVs^{-1}, 100 mVs^{-1}, and 200 mVs^{-1}) show that the greater the scan rate, the smaller the area of the CV curve. In addition, as seen in Figure 4.9, a comparison between the GCE and GCE-PANI CV tests shows that modification by coating PANI on the GCE surface increases the CV curve for the GCE-PANI sample. This increase in the CV curve indicates an increase in the electric field after modification.

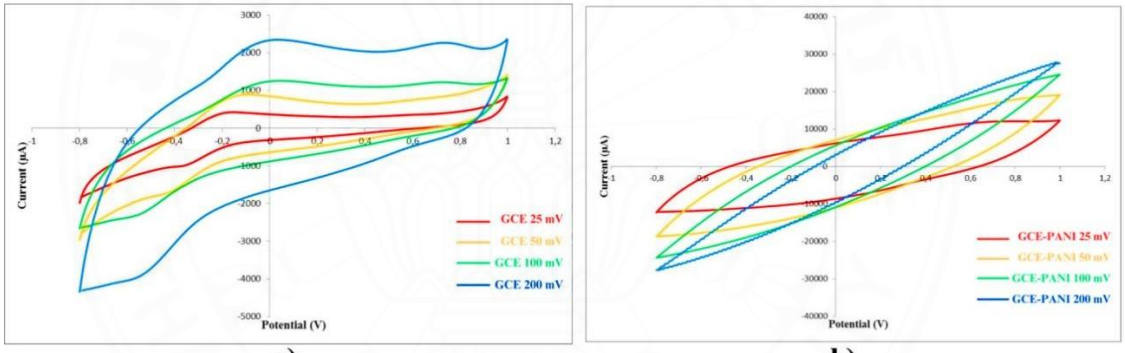

a) b)

Figure 4.8 The CV test of (a) GCE and (b) GCE-PANI

Ref. code: 25666422040920FRA

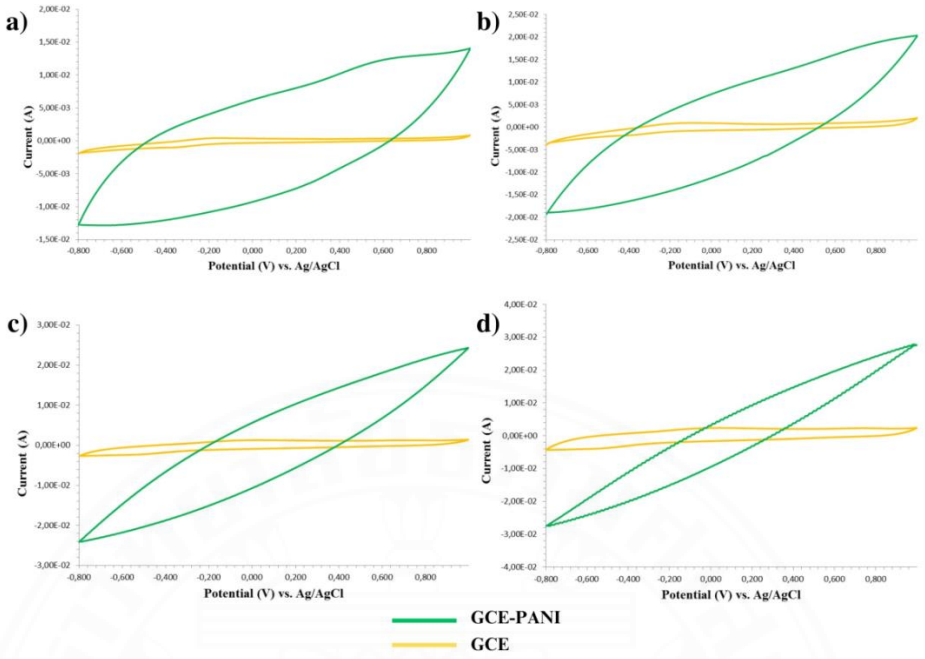

Figure 4.9 Comparison of CV test between GCE and GCE-PANI in each scan rates; (a) 25 mVs^{-1}, (b) 50 mVs^{-1}, (c) 100 mVs^{-1}, and (d) 200 mVs^{-1}

The specific capacitance of electrodes is calculated using the CV areas from Figure 4.8 following Equation 3.5. Figure 4.10 shows the measurements showing that GCE-PANI has a greater specific capacitance than GCE. The GCE's capacitance is effectively raised by the addition of PANI to it. However, when the scan rate increased, the specific capacitance of GCE-PANI decreased. Because the ions do not have enough time to interact with the electroactive species at higher scan rates, there may be a reduction in capacitance (Pandey et al., 2022).

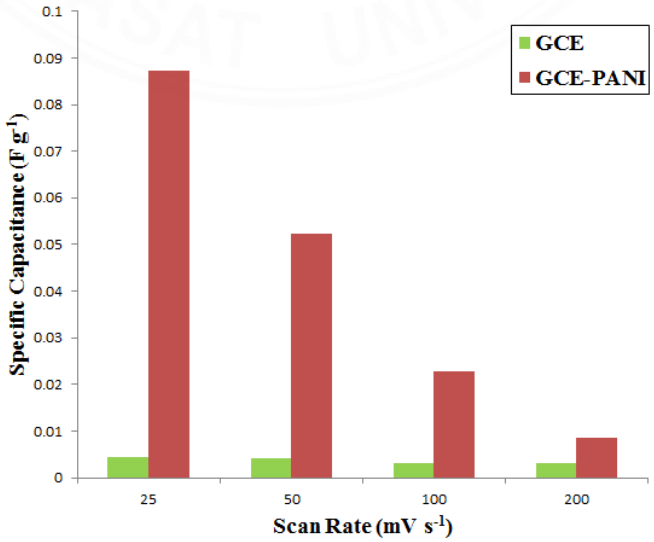

Figure 4.10 Specific capacitance of GCE vs. GCE-PANI

4.4 Modification of ACC

Figure 4.11 shows the shape of ACC before and after being modified with PANI coating. In contrast to the graphite samples, the PANI layer could not be seen clearly in the ACC. It took much work to distinguish the two ACC and ACC-PANI samples organoleptically. Instruments support from FTIR, FESEM, and BET prove the PANI coating on the ACC surface.

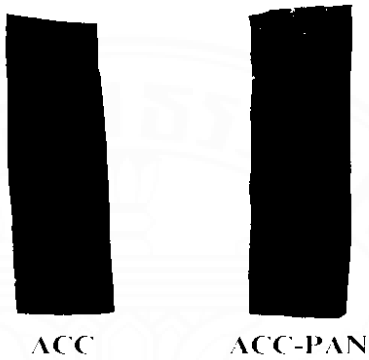

Figure 4.11 Unmodified ACC and ACC-PANI

4.4.1 FTIR Analysis of ACC-PANI

Based on the reaction illustrated in section 4.2, the electropolymerization process coated PANI on ACC. Figure 4.12 compares FTIR spectra from unmodified ACC and ACC-PANI. The peaks at 3242.86 cm^{-1} refer to the stretching of C−C bonding. The 1631.44 cm^{-1} peak demonstrated the existence of quinoid rings (Q) caused by the N=Q=N stretching vibration. The peak at 1131.60 cm^{-1} was due to PANI's C−N stretching mode. The peak at 1030.59 cm^{-1} belonged to the C−H in-plane bonding vibration. In contrast, the peak at 874.06 cm^{-1} is attributed to the C−H substituted in the aromatic ring. The S=O in-plane bending appears at 568.15 cm^{-1} (Shih et al., 2017; Zhang et al., 2021).

Ref. code: 25666422040920FRA

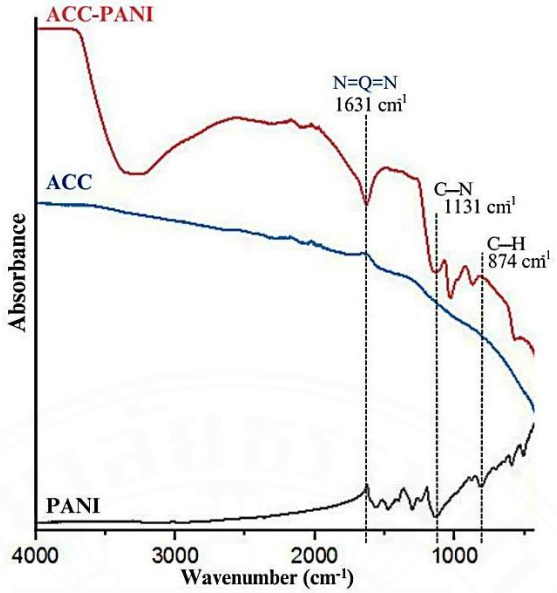

Figure 4.12 Comparison of FTIR between unmodified ACC and ACC-PANI

4.4.2 SEM Analysis of ACC-PANI

Surface micrographic characterization of the ACC and ACC-PANI electrodes was carried out using the FESEM instrument with 10000x magnification, as shown in Figure 4.13. The surface shape of the ACC electrode can be seen in Figure 4.13(a), resembling a smooth and fibrous surface. Physically, the shape of the ACC electrode is different from the GCE, where the GCE is in the form of a very dense cylindrical bar, while the ACC is in the form of a thin sheet. As a result, the structure seen at 10000x magnification appears to be a thin sheet similar to the structure of a leaf.

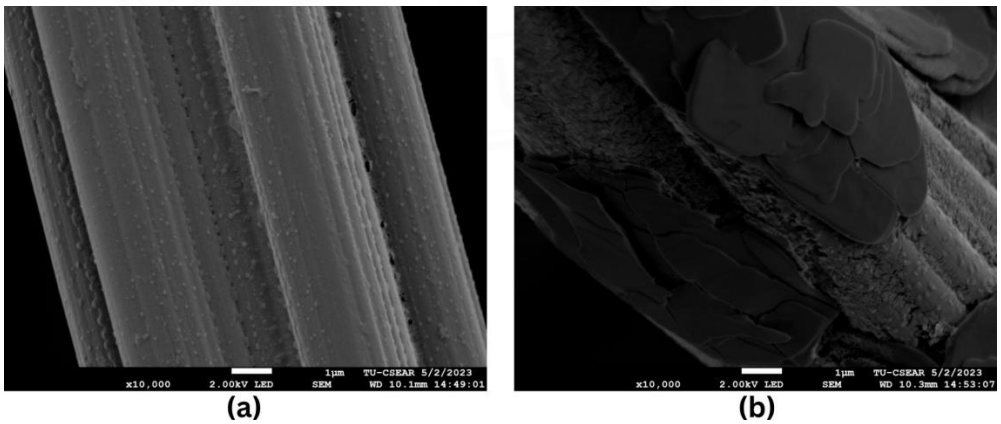

Figure 4.13 FESEM micrographs of (a) ACC; and (b) ACC-PANI

Figure 4.13(b) shows the surface morphology of the ACC-PANI electrode. The coating results on the ACC surface show a difference in the thickness of the

Ref. code: 25666422040920FRA

PANI layer formed. Additionally, the PANI on the ACC surface appears layer-like and denser in the FESEM pictures, making the pore structure less evident than on the PANI on GCE. This PANI coating's structure is comparable to that of the PANI coating studied by Narayanasamy & Jayaprakash (2021), which exhibits a thick, rough, and stable surface morphology.

The PANI layer formed appears to follow the morphology of the ACC surface, which appears smooth, in contrast to the GCE surface, which has an irregular structure. Furthermore, apart from having a different PANI layer thickness on each side, the coating results also show several sides of the ACC electrode that PANI does not cover. The uncovered side of ACC with PANI shows the uneven distribution of PANI formed on the ACC surface.

Rasyad and Arto (2018) explain that the current density is a value that states the amount of electric current flowing per unit area of the electrode surface. For this electrocoating process, the current density factor plays a crucial role because it will affect the efficiency of the coating, the oxidation-reduction reaction, and the diffusion of the resulting coating on the surface of the object being coated. Based on this explanation, the PANI coating process on the surface of the ACC electrode indicates a difference in conductivity between the ACC and GCE materials, resulting in a difference in the efficiency of the electropolymerization reaction. The difference in the ability of the electrodes to receive electric current, which affects the stability of the reaction, causes the formation of an uneven PANI layer with different thickness levels on several sides of the electrode. This result shows that the electropolymerization reaction on the ACC material has a lower effectiveness than the GCE material.

4.4.3 BET Analysis of ACC-PANI

Kajama et al. (2015) explained the graphical shape of the BET type I isotherm with the L-shape. The monomolecular adsorption equation by Langmuir helps explain the L-shape curve, a typical adsorption isotherm for diluted solutions over a solid/liquid interface—the L-shape curve indicates the microporous structure on the material's surface. Based on Figure 4.14, the N_2 gas adsorption graph on the BET test of the ACC and ACC-PANI materials shows an L-shape. So, referring to the theory

Ref. code: 25666422040920FRA

presented, the ACC and ACC-PANI electrodes' surface structure is porous with a micropore size smaller than 2 nm. The surface characteristics are shown in Table 4.3. However, ACC and ACC-PANI significantly reduced surface areas (1,193.52 and 222.34 m^2/g) and pore volumes (0.51 and 0.09 cm^3/g). This decline raises the possibility that the PANI layers obstruct the ACC's micropores due to the study by Haq et al. (2020), which indicates the potential of PANI chains to cover the porous structure on the pristine activated carbon and decrease its areas and volumes depending on their pore size distribution.

Table 4.3 Surface characteristics of ACC and ACC-PANI

Electrodes	BET Surface Area (m^2/g)	Pore Volume (cm^3/g)	Average Pore Size (Å)	Average Particle Size (Å)
ACC	1,193.52	0.51	16.89	50.02
ACC-PANI	222.34	0.09	16.37	263.49

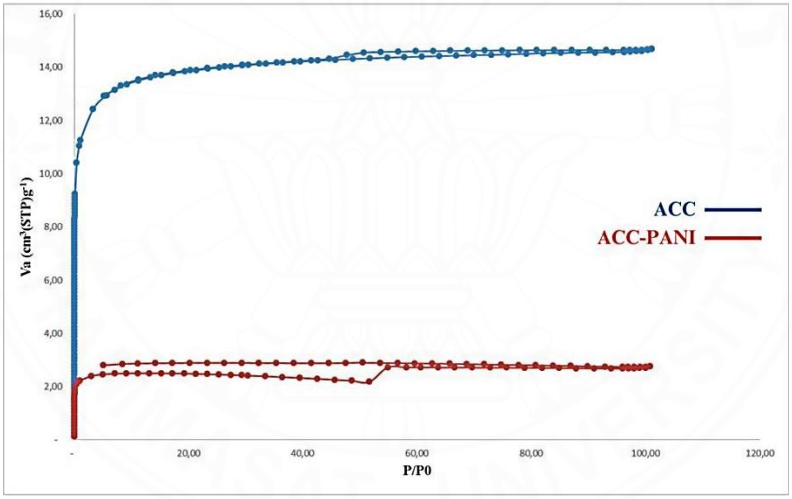

Figure 4.14 N_2 adsorption/desorption curve of ACC and ACC-PANI

4.4.4 Electrochemical Analysis of ACC-PANI

Figure 4.15 compares the results of the CV test for the analysis of electrochemical properties. The electrodes were subjected to a specific capacitance test using four successive scan rates of 5 mVs^{-1}, 10 mVs^{-1}, 15 mVs^{-1}, and 20 mVs^{-1}. Compared to the scan rate values used for the GCE and GCE-PANI sample tests, the variation in the scan rate test values for the ACC and ACC-PANI samples is more diminutive. Additionally, this shows that GCE and GCE-PANI are electrically superior to ACC and ACC-PANI. According to the test results for the ACC sample shown in Figure 4.15(a), the area of the voltammetric cyclic curve increased with

Ref. code: 25666422040920FRA

higher scan rates applied to the system. Contrary to the ACC-PANI test in Figure 4.15(b), it can be seen that the area of the cyclic voltammetric curve is getting smaller.

Figure 4.16 depicts the specific capacitance of ACC-PANI, which is less than that of ACC. The capacitance of ACC material cannot be increased by changing the PANI coating. This finding is normal and in line with the BET characterization, which showed that the presence of PANI on ACC caused the surface areas and pore volumes to decrease. Another researcher explained this occurrence, stating that an ACC material with these pore characteristics will inhibit the formation of an electric double layer, hence lowering the capacitance of the electrodes (Zakir et al., 2018).

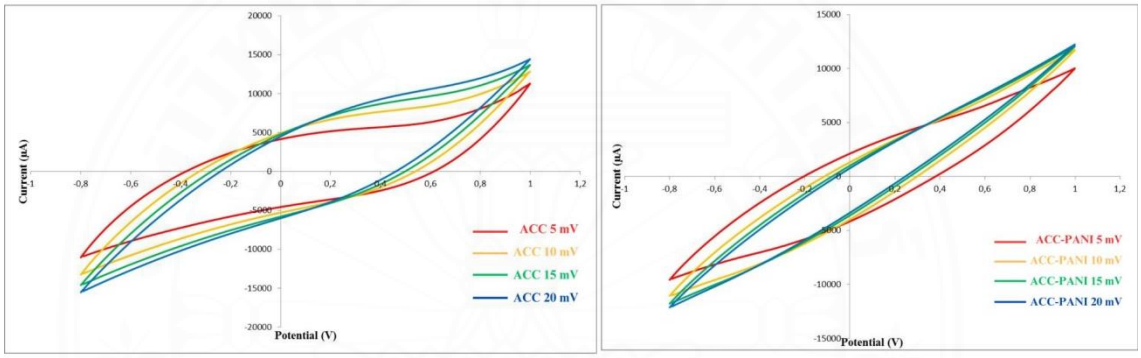

a) b)

Figure 4.15 The CV test of (a) ACC and (b) ACC-PANI

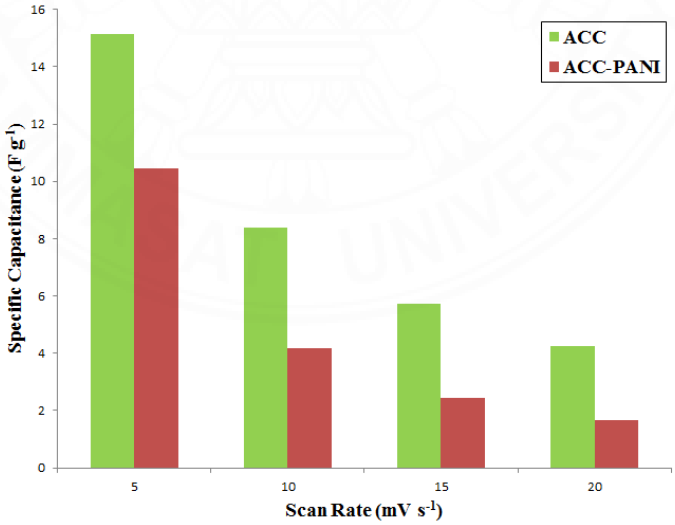

Figure 4.16 Specific capacitance of GCE vs. GCE-PANI

4.5 MFC Performances

Analysis of the production of electricity from the MFC system with anode without modification was carried out by calculating the amount of potential produced (V), electric current (A), current density (Acm^{-2}), and power density (Wcm^{-2}). There

Ref. code: 25666422040920FRA

are five kinds of MFC systems operated in this study, namely MFC with GCE anode (GCE MFC), MFC with ACC anode (ACC MFC), MFC with GCE-PANI anode (GCE-PANI MFC), MFC with ACC-PANI anode (ACC-PANI MFC), MFC with ACC-CT anode (ACC-CT MFC), and MFC with ACC-CT/PANI anode (ACC-CT/PANI MFC). Each system was tested using two electron acceptors: oxygen and ferricyanide. Except for the ACC-CT and ACC-CT/PANI, those two anodes were applied only in the oxygen system.

4.5.1 Electricity Generation on MFC with Oxygen

The MFC reactor was operated using a continuous flow of oxygen gas with a batch number of two cycles. Figure 4.17 shows a graph of the activity of measuring electrical energy generated from the GCE MFC vs. GCE-PANI MFC, and Figure 4.18 is the result of measuring electrical energy in the ACC MFC vs. ACC-PANI MFC. Based on the measurement results, the second cycle of the two systems gave better results. In addition, regarding operational time, the second operating cycle shows more prolonged work activities than the first. This activity could be due to better bacterial growth and biofilm formation than in the first cycle. Table 4.4 shows the operating time of the reactor with the four different anode systems.

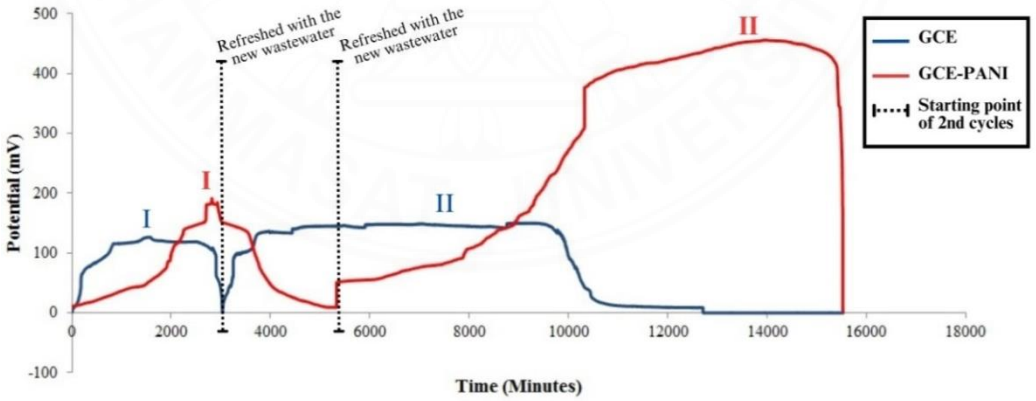

Figure 4.17 Potential generated at 500 Ω resistor in O_2-based GCE MFC

Ref. code: 25666422040920FRA

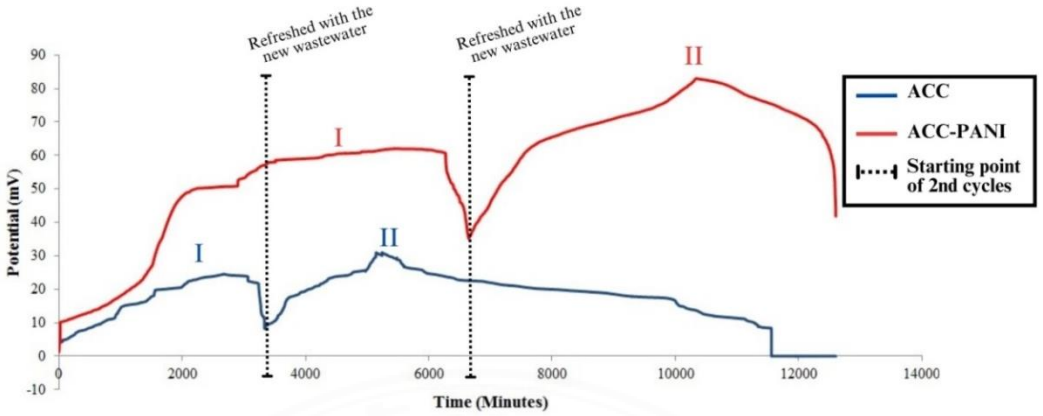

Figure 4.18 Potential generated at 500 Ω resistor in O_2-based ACC MFC

Table 4.4 Operational duration of MFC with Oxygen

Reactor System	Duration Cycle I	Duration Cycle II
GCE	50 hours 30 minutes	160 hours 38 minutes
GCE-PANI	88 hours 10 minutes	170 hours 40 minutes
ACC	55 hours 50 minutes	136 hours 47 minutes
ACC-PANI	107 hours 20 minutes	102 hours 31 minutes

Based on the graph of the rate of electricity production from the two MFC systems in Figure 4.17 and Figure 4.18 above, the results show that the MFC system with modified anodes has higher electricity production than the pure anodes. The highest electricity production for systems with graphite materials, GCE and GCE-PANI, was recorded at 150.25 mV and 455.88 mV, respectively. The average potential is measured as long as the system operates 103.99 mV for the GCE system and 207.22 mV for the GCE-PANI system. This result is very different compared to a system made of carbon cloth. The highest potential measurements recorded during the two operating cycles were 30.99 mV for the ACC system and 82.99 mV for the ACC-PANI system, with an average measured value of 18.76 mV and 57.07 mV, respectively. A statistically significant increase (t-test, $P < 0.05$) was observed in the increase in electricity production in MFC GCE-PANI compared to MFC GCE and MFC ACC-PANI as compared to MFC ACC.

The difference in results is expected, considering the different characteristics of the two materials. One of the factors that dramatically influences the two materials to produce different results is the morphology of the surface structure. The pore structure's morphology on the electrode's surface can affect the biofilm formation process and impact the biocompatibility of the material and the resulting electricity

Ref. code: 25666422040920FRA

production. Greenman et al. (2021) explained that a conductive polymer such as polyaniline or polypyrrole with graphene materials used in electrode construction could reduce geometric constraints. Reducing the geometric constraints will have an impact on the effectiveness of the electrode in the formation of biofilms with bacterial activity. *Graphite* is a carbon material composed of graphene layers. So, in this study, the GCE material, if its surface were modified using PANI, would be far more profitable and give better results.

MFC testing in this oxygen system was also carried out using an ACC anode with carbon tape (CT) added to the surface before being modified with PANI coating. MFC test results with ACC-CT vs. ACC-CT/PANI are shown in Figure 4.19. Results show that the maximum MFC performance is produced by the ACC-CT/PANI anode with almost three times higher electricity than ACC-CT. The resulting potential is 125.0 mV for the ACC-CT/PANI reactor and 48.74 mV for the ACC-CT reactor. These results are similar to the MFC operated using pure ACC-based anodes (without adding CT), presented in Figure 4.18. The electricity production of MFC from ACC vs. ACC-PANI and ACC-CT vs. ACC-CT/PANI showed that the addition of CT did not significantly affect the conductivity of the ACC material.

Polarization tests were carried out on ACC-CT and ACC-CT/PANI reactors with several variations of resistors ranging from 1 ohm to 10,000 ohms. The results of the polarization test are shown in Figure 4.20. The internal resistance of the MFC is calculated considering the slope of the overall polarization curve. Figure 4.20(a) shows the potential vs. tested external resistor polarization curve. The polarization test shows that the greater the value of the external resistor, the greater the potential generated. Figure 4.20(b) between potential vs. the current density shows a maximum current density of 2.70×10^{-3} A m^{-2}.

Ref. code: 25666422040920FRA

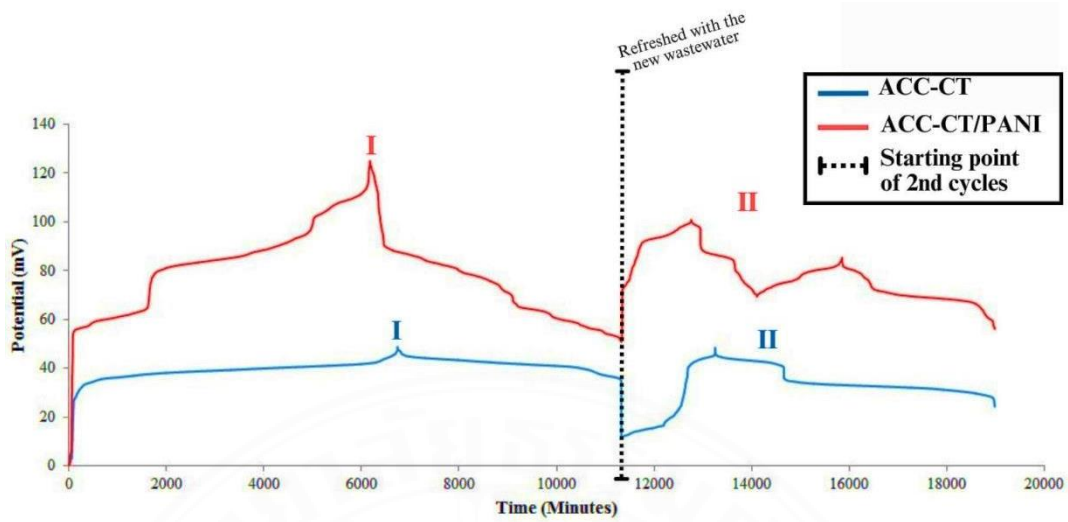

Figure 4.19 Potential generated at 10,000 Ω resistor in O_2-based ACC-CT MFC

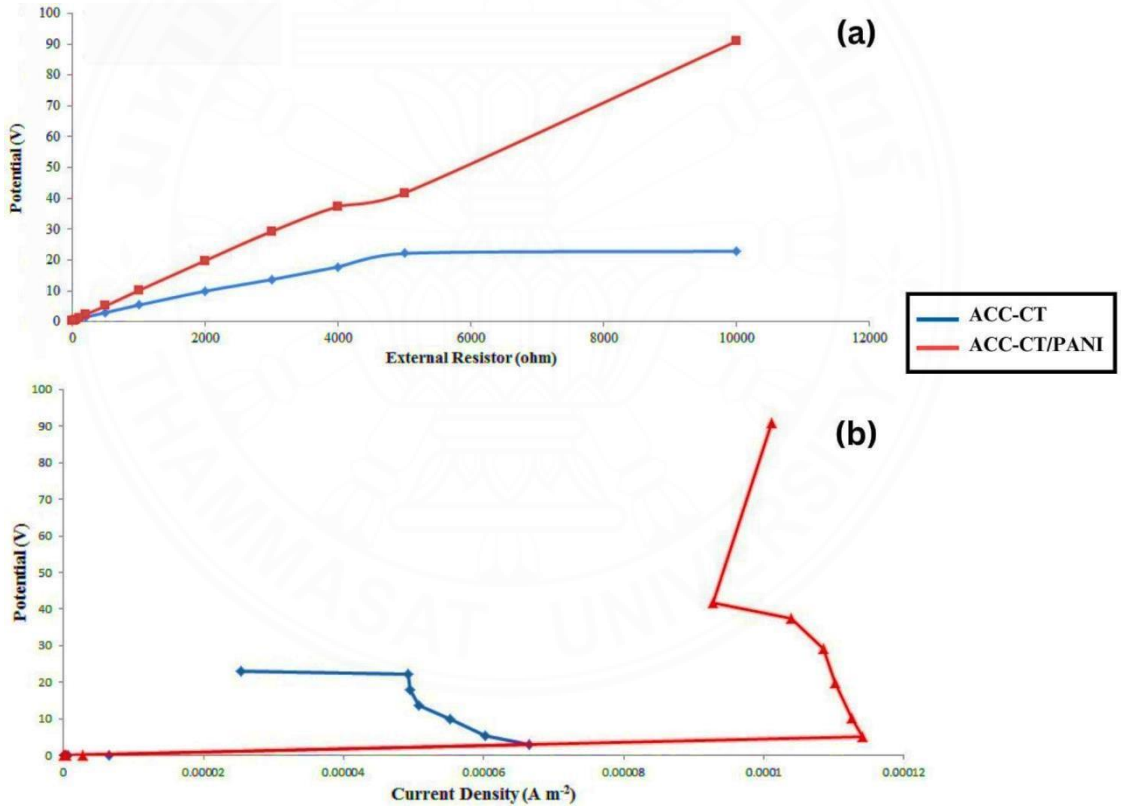

Figure 4.20 Polarization curve of: (a) Potential vs. External Resistor; and (b) Potential vs. Current Density

MFC electricity generation is strongly influenced by electrode morphology and bacterial activity. Furthermore, Siagian et al. (2017) also explained the formation of biofilms on the surface of graphite rods, where biofilms grow and spread across the surface of the carbon rods thickly. The nature of the spread of this biofilm gives an advantage to the efficiency of the MFC because it can affect the number of electrons

Ref. code: 25666422040920FRA

transferred from the anode. The analysis and calculation results of current density and power density are shown in Table 4.5, which compares electricity production from the four types of anode materials used. Figure 4.21 provides a current density comparison between all electrodes at every minute.

Table 4.5 Power density and current density of MFC system with oxygen

MFC Systems	Power Density (W cm^{-2})		Current Density (A cm^{-2})	
	Maximum	**Average**	**Maximum**	**Average**
GCE	9.03×10^{-7}	4.42×10^{-7}	6.01×10^{-6}	3.40×10^{-6}
GCE-PANI	1.41×10^{-5}	4.81×10^{-6}	3.09×10^{-5}	1.40×10^{-5}
ACC	3.84×10^{-8}	4.66×10^{-7}	1.24×10^{-6}	5.62×10^{-6}
ACC-PANI	1.41×10^{-8}	2.44×10^{-7}	6.88×10^{-7}	3.86×10^{-6}
ACC-CT	2.64×10^{-9}	1.57×10^{-9}	5.42×10^{-8}	4.09×10^{-8}
ACC-CT/PANI	1.74×10^{-8}	7.08×10^{-9}	1.39×10^{-7}	8.71×10^{-8}

Based on the data presented in Table 4.5, MFCs that are operated using electrodes made of graphite, either pure or modified with polymer coating, can produce better energy production. The best result from the MFC system using oxygen as the electron acceptor is with GCE-PANI material as the anode. These results support the theory presented in Section 2.4.2, where PANI is said to be a type of polymer capable of increasing the biocompatibility properties of materials and supporting the growth of electro-active bacteria. The highest power density results from the MFC system with GCE-PANI is 1.41×10^{-5} Wcm^{-2} with an average calculated production of 4.81×10^{-6} Wcm^{-2}. The current density is 1.40×10^{-5} Acm^{-2} with a maximum measured result of 2.09×10^{-5} Acm^{-2}.

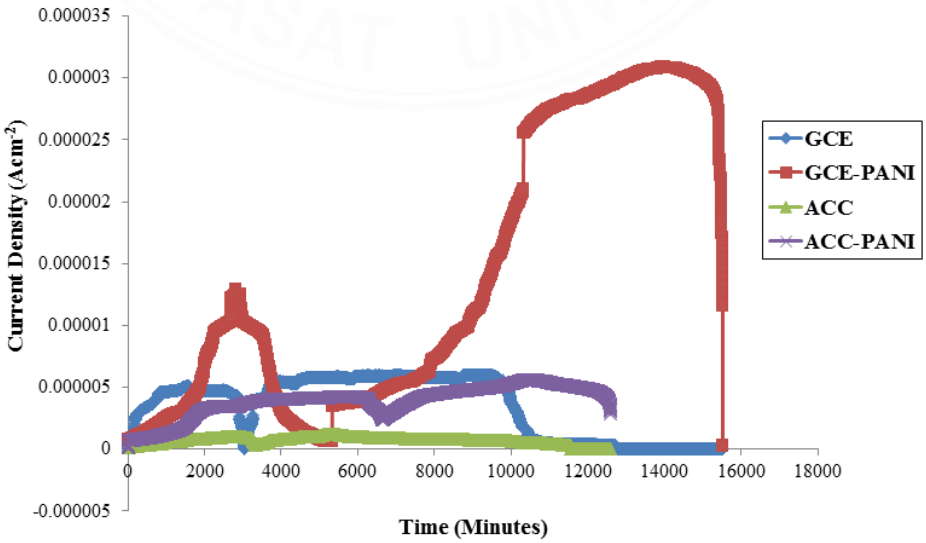

Figure 4.21 Current density vs. time between all electrodes at 500 Ω resistor with O_2

Ref. code: 25666422040920FRA

4.5.2 Electricity Generation on MFC with Ferricyanide

The second system in this study operates MFC using ferricyanide as an electron acceptor. The ferricyanide ion is obtained from a $K_3[Fe(CN)_6]$ electrolyte solution in the cathode chamber. As with the MFC system with oxygen, this section will also compare the performance of the MFC in producing electricity from the four types of anodes used. Based on the results of potential measurements shown in Figure 4.22 for graphite-based anodes and Figure 4.23 for carbon cloth-based anodes, there appears to be an increase in energy production by using ferricyanide as an electron acceptor.

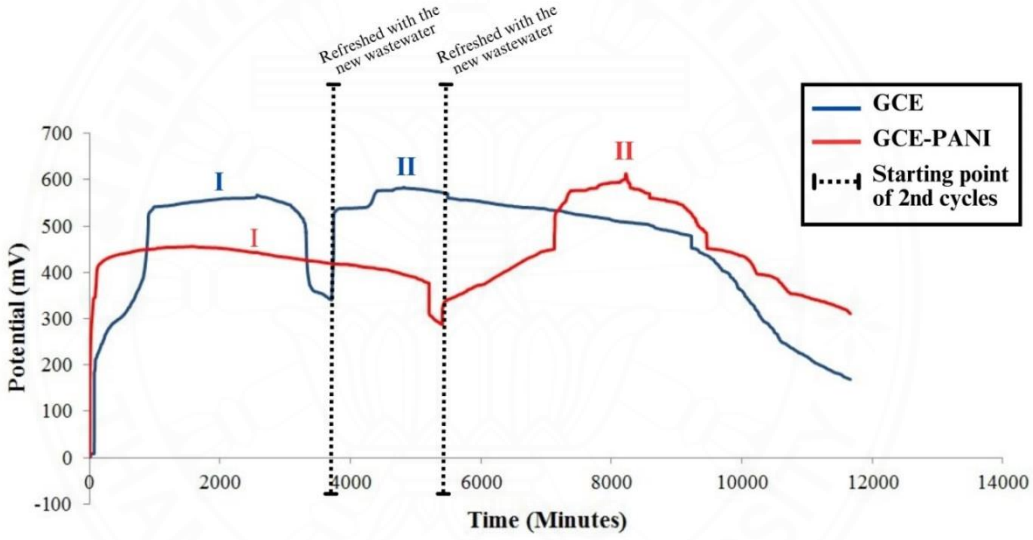

Figure 4.22 Potential generated at 500 Ω resistor in $K_3[Fe(CN)_6]$-based GCE MFC

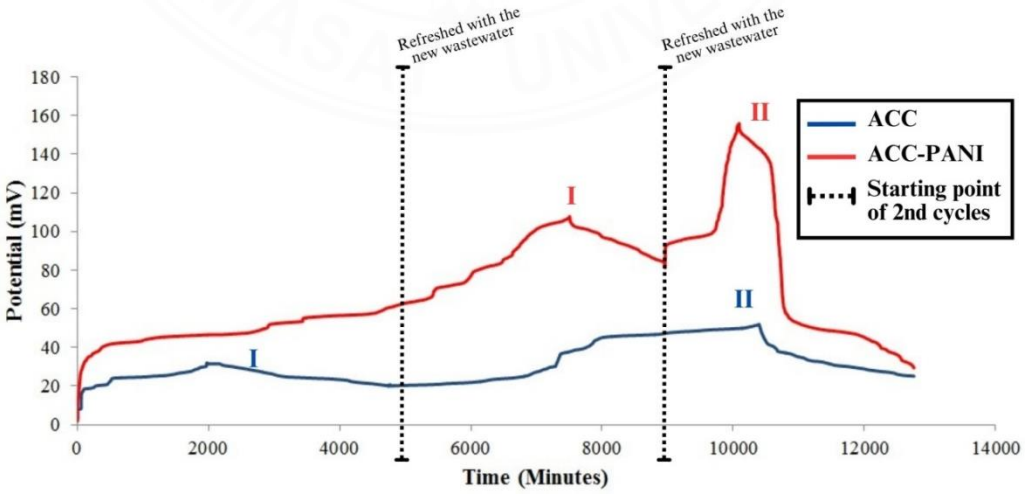

Figure 4.23 Potential generated at 500 Ω resistor in $K_3[Fe(CN)_6]$-based ACC MFC

Ref. code: 25666422040920FRA

The test results show that graphite-based anodes can produce better electricity than carbon-based anodes. The maximum measured voltage of the system with ACC is 51.95 mV, with an average measurement of 30.88 mV. The polymer modification results on the ACC-PANI anode are indeed considered capable of increasing electricity production, and this can be seen in Figure 4.23, where the maximum measured voltage can reach 155.95 mV with an average measurement of 70.29 mV. These increment in electricity production of MFC ACC-PANI against MFC ACC showed a statistically significant increase (t-test, $P < 0.05$). However, these results are still relatively small compared to measurements using GCE and GCE-PANI as anodes. Based on Figure 4.22, it is known that using pure GCE, the highest voltage that can be measured is 583.97 mV, with an average measurement of 464.24 mV. Based on this comparison, it can be seen that the anode material made from graphite has much better effectiveness and ability to generate electricity when compared to materials made from carbon cloth, even though the carbon cloth has been modified with a polymer coating which can improve its biocompatibility properties and support bacterial growth but is still not able to produce better electricity production than pure graphite anode material.

As for Figure 4.22 regarding the comparison of electricity production between GCE and GCE-PANI in the MFC system with ferricyanide, it can be seen that in the first operational cycle, GCE-PANI produces lower electricity production when compared to systems using pure GCE. The MFC reactor, operated using pure GCE in its first cycle, produced the highest measured voltage of 566.92 mV with an average production of 466.32 mV. Meanwhile, the results of measurements using GCE-PANI in the first cycle were only able to obtain the highest voltage in the range of 455.88 mV with an average production of 422.79 mV. Although the measurement results in the first cycle between the two graphite-based anodes show lower GCE-PANI performance than GCE, these results align with relatively normal.

Acclimatization factors and the formation of biofilms in the MFC reactor itself strongly influenced the lower performance of GCE-PANI in its first cycle. In the GCE test using ferricyanide, the reactor used is the same reactor that GCE operates when using oxygen. The replacement of the electron acceptor from oxygen to ferricyanide at the cathode vessel is carried out directly without changing the GCE and the system

Ref. code: 25666422040920FRA

in the anode chamber. While the operation using GCE-PANI in ferricyanide uses a new reactor, the system must re-acclimatize and build suitable environmental conditions for electroactive bacteria to grow. Therefore, referring to the explanation regarding the effect of biofilm formation on MFC performance presented in Section 4.5.1, the GCE operation on ferricyanide using the same reactor with an oxygen system has adequate biofilm and suitable environmental conditions in the anode chamber for growth and activity of electroactive bacteria. This condition resulted in the operation of the first cycle that GCE performed better than GCE-PANI.

However, the first cycle of MFC with GCE-PANI is considered capable of providing better stability to the system compared to GCE, and this can be seen from Figure 4.22, where GCE-PANI has a longer operational time. Furthermore, in the second cycle of these two types of electrodes, electricity production from GCE-PANI has increased compared to the first cycle. This result is inversely proportional to the MFC system that uses GCE because the electricity production generated between the first and second cycles shows an insignificant increment. A comparison of operational time and measurement of power density and current density is shown in Tables 4.6 and 4.7, respectively. The MFC with GCE-PANI generated higher electricity than others. It also can be seen from Figure 4.24 provided a current density comparison between all electrodes at every minute.

Table 4.6 Operational duration of MFC with $K_3[Fe(CN)_6]$

Reactor System	Duration Cycle I	Duration Cycle II
GCE	61 hours 54 minutes	132 hours 31 minutes
GCE-PANI	90 hours 11 minutes	104 hours 14 minutes
ACC	76 hours 46 minutes	132 hours 54 minutes
ACC-PANI	146 hours 26 minutes	63 hours 14 minutes

Table 4.7 Power density and current density of MFC system with $K_3[Fe(CN)_6]$

MFC Systems	Power Density (W cm^{-2})		Current Density (A cm^{-2})	
	Maximum	Average	Maximum	Average
GCE	1.36×10^{-5}	9.26×10^{-6}	2.34×10^{-5}	1.86×10^{-5}
GCE-PANI	2.54×10^{-5}	1.34×10^{-5}	4.15×10^{-5}	2.97×10^{-5}
ACC	1.08×10^{-7}	4.21×10^{-8}	1.34×10^{-7}	1.24×10^{-6}
ACC-PANI	1.65×10^{-8}	3.91×10^{-7}	1.05×10^{-6}	4.76×10^{-6}

Ref. code: 25666422040920FRA

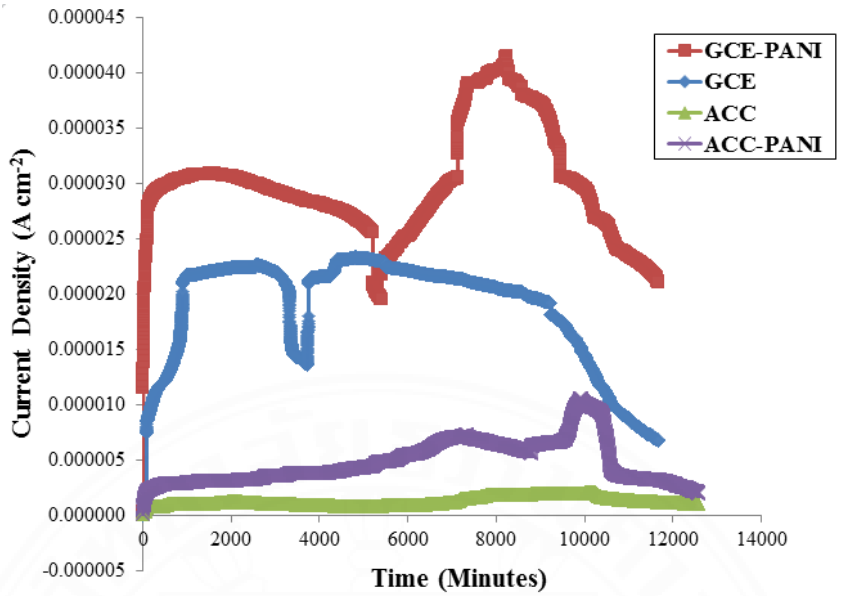

Figure 4.24 Current density vs. time between all electrodes at 500 Ω resistor with $K_3[Fe(CN)_6]$

4.6 Comparison of Electricity Generated in O_2 and $K_3[Fe(CN)_6]$ vs. Other Studies

Based on the explanations in Sections 4.5.1 and 4.5.2 regarding the production of electricity generated from the four types of anodes used for two types of electron acceptors, it can be seen that systems with ferricyanide ions as electron acceptors can generate higher electricity. The difference in the ability of ferricyanide and oxygen to capture electrons and generate electricity is presented in Figures 4.17, 4.18, 4.19, 4.22, and 4.23. One of the comparisons is the production potential between the MFC and the GCE-PANI anode operated in a reactor with oxygen and ferricyanide. In the GCE-PANI MFC with oxygen, the maximum power density measured was 1.41×10^{-5} Wcm^{-2}, while in the system with ferricyanide, the maximum power density obtained was 2.54×10^{-5} Wcm^{-2}. Based on this comparison, it can be seen that the ferricyanide as an electron acceptor in this reactor can increase the MFC performance up to 80.14%.

The results of comparing the power density of GCE-PANI with oxygen and ferricyanide align with the theory previously described in Section 2.3.1. Ferrycyanide is reported as an electroactive species that can capture electrons very well and has a low overpotential so that it can produce a faster reaction with a greater energy output. Furthermore, Ucar et al. (2017) have also stated that carbon materials, when operated

Ref. code: 25666422040920FRA

with ferricyanide, were able to produce 50−80% better power. Another study using ferricyanide as an electron acceptor was carried out by Faria et al. (2017), who operated a dual-chamber MFC using substrates from the dairy industry's wastewater. The study obtained the highest power density of 9.2×10^{-2} Wcm^{-2} using electrodes made of stainless steel, which has a higher conductivity than the carbon-based materials in this study.

4.7 Wastewater Analysis

4.7.1 Treatment Efficiencies

Based on Table 4.8, MFC is very effective in handling wastewater. The test results show that the efficiency level of COD reduction in wastewater using MFC reaches more than 80%. Additionally, according to the treatment efficiencies, the COD elimination after the second operation cycle is more incredible than during the first cycle. According to these findings, microorganisms have a better capacity to break down organic matter the longer their reaction time is. Additionally, Table 4.8 demonstrates that MFC with PANI-coated electrodes performed better with high COD removal. These findings suggest that altering the polyaniline layer can increase the biocompatibility of the electrode material. The PANI coating on the GCE and ACC surfaces has a positive impact on bacterial development, which can decrease the COD levels in wastewater with a sufficient level of efficiency, which are 88.8% for the MFC with GCE-PANI anode and 89.7% for the ACC-PANI anode.

Table 4.8 COD removal efficiencies using with and without anode modification in MFC system

System of MFC	Treatment Efficiency (%Removal)			
	with Oxygen		with Ferricyanide	
	Cycle 1	Cycle 2	Cycle 1	Cycle 2
GCE	85.3	87.7	83.2	85.3
GCE-PANI	82.1	85.8	82.1	88.8
ACC	84.8	87.3	82.6	84.2
ACC-PANI	81.6	89.7	82.1	87.2
ACC-CT	80.9	81.3	-	-
ACC-CT/PANI	84.6	84.1	-	-

Some MFCs are also reported to treat wastewater and sludge from the brewery industry. A study from Ghana reported that MFC can remove COD content from

Ref. code: 25666422040920FRA

brewing industry wastewater with an efficiency of up to 86.98%. The study was operated by a pot-shaped earthenware reactor with an anodic chamber in the center. This type of reactor is reported to exhibit high COD removal efficiency because the pot-shaped reactor functions as an anode chamber and a membrane surrounding the entire reactor. Pots made of clay are reported to have a porous structure. When applied as an anode chamber and an MFC membrane, the degradation, production, and electron transfer processes become more extensive than the reactor form used in this study. In addition, the wastewater used is directly from the brewery industry with the addition of H_2O_2 (Tamakloe et al., 2015). The use of H_2O_2 is reported to affect the increase in the reduction of COD in wastewater (Beyazit & Atmaca, 2021). In contrast, this study only used the UASB sludge to acclimate bacteria in the anode chamber. A comparison of several studies related to the wastewater treatment of the brewery industry is reported in Table 4.9.

Table 4.9 shows that in several similar systems, reducing COD in this study has yielded better results than in previous studies. The study conducted by Negassa et al. (2021) using GCE as an electrode and ferricyanide as an electron acceptor gave the highest COD reduction of 83%. This study used the same type of electrode, namely pure GCE with ferricyanide, giving a yield of 85.3%, and replacing it with a modified GCE-PANI anode increased the efficiency of COD removal, reaching 88.8%. What differentiates the two studies is the type of membrane used to separate the two sides of the reactor. However, this does not rule out the results that PANI modification on the GCE surface can increase the effectiveness of MFC performance in wastewater management.

Table 4.9 Comparison of COD removal of brewery wastewater treated in MFC

Wastewater	MFC type	COD Removal	Reference
Brewery wastewater	Pot-shaped earthenware reactor	86.98%	Tamakloe et al. (2015)
Synthetic with brewery sludge	Dual-chamber with salt bridge and GCE electrodes. Electron acceptor was ferricyanide.	79 – 83 %	Negassa et al. (2021)
Synthetic with brewery sludge	Dual-chamber with CEM and carbon fiber cloth electrodes	71%	Yahampath Arachchige Don et al. (2021)

Ref. code: 25666422040920FRA

Wastewater	MFC type	COD Removal	Reference
Brewery wastewater	Single-chamber MFC with	87.1%	Kumar et al. (2019)
Synthetic with brewery sludge	Dual-chamber with CEM and GCE-PANI as anode and GCE as cathode	• 88.8% (in ferricyanide) • 85.8% (in oxygen)	This study
Synthetic with brewery sludge	Dual-chamber with CEM and ACC-PANI as anode and ACC as cathode	• 87.2% (in ferricyanide) • 89.7% (in oxygen)	This study

4.7.2 Normalized Energy Recovery (NER) and Current Efficiency (CE)

NER is an alternative way to present energy generated from MFC. The two units used to express NER are NER_V in kWh m^{-3}, which is based on the amount of wastewater that has been treated in the MFC, and NER_{COD} in kWh $kgCOD^{-1}$, which is based on the volume of organic substrate that has been measured as the chemical oxygen demand reduced in the MFC. According to Xiao et al. (2014), *kWh* is used in NER rather than *kJ* to share research findings between academia and industry more effectively. *kWh* is a unit that is frequently used in the wastewater sector. The NER calculation is reported in Table 4.10.

Table 4.10 NERand CE of MFC in oxygen and ferricyanide systems

Anodes	Oxygen Systems				
	NER_V (kWh m^{-3})		NER_{COD} (kWh $kgCOD^{-1}$)		Current Efficiency (%)
	Cycle 1	Cycle 2	Cycle 1	Cycle 2	
GCE	4.57×10^{-10}	2.53×10^{-5}	1.34×10^{-7}	7.21×10^{-2}	3.8
GCE-PANI	1.30×10^{-7}	3.94×10^{-4}	3.95×10^{-5}	1.13×10^{-1}	14.1
ACC	2.58×10^{-8}	2.62×10^{-6}	7.59×10^{-6}	8.04×10^{-4}	0.7
ACC-PANI	9.22×10^{-7}	7.46×10^{-6}	2.64×10^{-4}	2.08×10^{-3}	2.1
ACC-CT	4.82×10^{-9}	5.28×10^{-8}	1.49×10^{-6}	1.62×10^{-5}	0.1
ACC-CT/PANI	1.18×10^{-7}	3.47×10^{-7}	3.47×10^{-5}	1.03×10^{-4}	0.3
Anodes	**Ferricyanide Systems**				
	NER_V (kWh m^{-3})		NER_{COD} (kWh $kgCOD^{-1}$)		Current Efficiency (%)
	Cycle 1	Cycle 2	Cycle 1	Cycle 2	
GCE	5.79×10^{-5}	3.27×10^{-4}	1.74×10^{-2}	2.73×10^{-2}	18.7
GCE-PANI	8.96×10^{-5}	4.07×10^{-4}	9.59×10^{-2}	1.15×10^{-1}	19.6
ACC	1.98×10^{-7}	1.46×10^{-5}	5.99×10^{-5}	4.45×10^{-3}	17.9
ACC-PANI	2.59×10^{-6}	1.98×10^{-5}	7.69×10^{-4}	5.67×10^{-3}	25.9

Ref. code: 25666422040920FRA

Table 4.10 presents NER_V and NER_{COD} calculation data from all tested MFC systems. The comparison of NER values is considered very suitable for cross-comparing various MFCs made for wastewater treatment because it does not consider reactor size and has data on wastewater flow rate and organic removal efficiency. In addition, presenting NER data will help create an energy balance in MFCs, which can highlight knowledge and development gaps for MFCs to be energy-efficient or profitable processing technologies. Based on these data, it was found that in all MFC systems tested with oxygen and ferricyanide, there was an increase in energy production in reactors operated using modified GCE-PANI and ACC-PANI anodes. The increase in energy is also seen to occur significantly in the second operating cycle. Especially on the NER_{COD} value, which is based on the amount of COD degraded, the reactor with GCE-PANI showed NER_{COD} results in the oxygen and ferricyanide systems of 0.115 and 0.146 kWh $kgCOD^{-1}$, respectively.

The CE value in percent is also presented in Table 4.10. Based on the measurement, the results proved that modification of the carbon anode using PANI could increase the current efficiency of the MFC reactor. Percent current efficiency shows the proportion of the total power used to achieve the intended electrolytic reaction (Natarajan, 1985). MFCs with oxygen as an electron acceptor tend to have low CE values. These results align with the potential generated previously explained in Figures 4.22 and 4.23 that MFC with oxygen produces lower energy than ferricyanide. The best CE from the oxygen system was with GCE-PANI. CE value for the GCE anode was 3.8%, which increased after the modification to 14.1% for GCE-PANI. The results for the system with ferricyanide obtained a relatively high CE value. The CE value of MFC with the GCE anode was 18.7% and slightly increased to 19.6% for the GCE-PANI anode. The increase in CE value for the graphite-based anode tends to be low compared to the increase in the carbon cloth-based anode, where the ACC anode has a CE value of 17.9% and increases to 25.9% for ACC-PANI. Based on the potential generated by all MFCs, the electricity between GCE-PANI and GCE for ferricyanide did not experience a significant increase, so the increase in its CE was relatively low. In contrast, the ACC-PANI has a significant electricity increase, proving a higher increase in the CE for the ACC-PANI anode.

Ref. code: 25666422040920FRA

Based on the reactor's design and the electrode's shape, Samsudeen et al. (2015) examined the performance of MFC under various circumstances. The MFCs were operated in dual-chamber, triple-chamber, and multi-chamber reactors. The CE assessed were 6.7% for a dual-chamber MFC, 12.9% for a triple-chamber MFC, and 8.8% for a multi-chamber MFC. Graphite electrodes in plate and cylinder forms were utilized, producing 7.7% and 5.1% CE values, respectively. Another study by Yang et al. (2020) used activated carbon electrodes to process synthesis wastewater in a single chamber MFC reactor with an external resistance of 1000 ohms, yielding a CE of 13 ± 0.2%. Those two studies revealed that the CE analysis conducted for this study had generally positive findings. The use of graphite cylinder electrodes in this study reached CE up to 19.6%, while the other study can only reach CE of 5.1%. The modification of PANI coating on the GCE and ACC surfaces demonstrated the value of MFC in boosting electricity production and wastewater treatment efficiencies.

4.8 Salt Analysis and Identification

In operating the MFC, salt formation has been observed to occur on the surface of the anode chamber, as shown in Figure 4.25. This observation indicates the oxidation reaction from the wastewater treated with MFC. Identification of the types of mineral salts and their concentration analysis is presented in Table 4.11. This analysis found four oxidized ionic minerals with the highest-concentrated is for sodium salt, with a concentration of 6.31 mg L^{-1}. Oxidation of some minerals that occur during the MFC running process is normal. It does not affect the operating performance of the MFC. Based on the types of metals identified from the results of this analysis, namely sodium, potassium, calcium, and magnesium, which, if viewed theoretically based on the voltaic cell series activity, the four metals are included in the group of metals that are relatively easy to oxidize.

Ref. code: 25666422040920FRA

Figure 4.25 Salts on the surface of the anode chamber

Table 4.11 ICP analysis of oxidized salt on reactor surface

Oxidized salt	Concentration (mg L^{-1})
Na	6.31
K	1.48
Ca	0.07
Mg	0.08

Ref. code: 25666422040920FRA

CHAPTER 5
CONCLUSION AND RECOMMENDATION

5.1 Conclusions

As an environmental technology that optimizes the performance of electroactive bacteria in wastewater treatment, MFC shows outstanding performance. Following the research objectives, two aspects can be studied from this research.

1. Modifying GCE and ACC materials with PANI coating is the right step in improving MFC performance. PANI is proven as a type of polymer that can improve the conductivity and biocompatibility properties of GCE and ACC materials. Based on the characterization of material properties, the PANI layer provides a more favorable pore structure at the anode. In general, GCE-PANI has superior physical characteristics compared to ACC-PANI. This result can be seen from the electrochemical analysis results and GCE-PANI's ability to generate electricity from the MFC.
2. Differences in electron acceptors indicate differences in electricity production results. The highest electrical energy was obtained from the system using ferricyanide as an electron acceptor with the highest power density of 2.54×10^{-5} W cm^{-2} and a voltage of 612.81 mV for MFC GCE-PANI. As for the MFC with ACC-PANI anode, it produced a power density of 1.65×10^{-8} W cm^{-2} and 155.951 mV. MFC with GCE-PANI as the anode can generate four times more electricity than ACC-PANI.
3. Reviewing the ability of MFC to degrade COD content in wastewater, in this study, there was no significant difference in the ability of each MFC system to degrade COD. Overall, the treatment efficiency of all tested MFC systems reached more than 80%, with the highest efficiency being 88.8% of MFC with GCE-PANI in the second operational cycle with ferricyanide and 89.7% from MFC with ACC-PANI in the second operational cycle with oxygen.

5.2 Recommendation

Several developments can be made to improve this research in the future. First, GCE and ACC materials can be modified with other polymers to compare their

Ref. code: 25666422040920FRA

performance with polyaniline, or composites can be made by coating the metal on the surfaces of GCE-PANI and ACC-PANI so that it is expected to increase the conductivity of the materials further. The second recommendation is to test and analyze the bacterial species in the UASB sludge used. Because the bacteria used in this study are mixed culture colonies, it will be complicated to identify if a problem arises in the mixed culture system. In addition, by identifying and analyzing bacteria, it is easy to identify the effect of the biofilm formed and its effect on the resulting electricity production.

Ref. code: 25666422040920FRA

REFERENCES

Aelterman, P., Rabaey, K., Pham, H. T., Boon, N., & Verstraete, W. (2006). Continuous Electricity Generation at High Voltages and Currents Using Stacked Microbial Fuel Cells. *Environmental Science & Technology*, *40*(10), 3388–3394. https://doi.org/10.1021/es0525511

Aelterman, P., Versichele, M., Marzorati, M., Boon, N., & Verstraete, W. (2008). Loading rate and external resistance control the electricity generation of microbial fuel cells with different three-dimensional anodes. *Bioresource Technology*, *99*(18), 8895–8902. https://doi.org/10.1016/j.biortech.2008.04.061

Ahirrao, D. J., Pal, A. K., Singh, V., & Jha, N. (2021). Nanostructured porous polyaniline (PANI) coated carbon cloth (CC) as electrodes for flexible supercapacitor device. *Journal of Materials Science & Technology*, *88*, 168–182. https://doi.org/10.1016/j.jmst.2021.01.075

Ahn, Y., Zhang, F., & Logan, B. E. (2014). Air humidity and water pressure effects on the performance of air-cathode microbial fuel cell cathodes. *Journal of Power Sources*, *247*, 655–659. https://doi.org/10.1016/j.jpowsour.2013.08.084

Ashokkumar, S. P., Vijeth, H., Yesappa, L., Niranjana, M., Vandana, M., & Devendrappa, H. (2020). Electrochemically synthesized polyaniline/copper oxide nano composites: To study optical band gap and electrochemical performance for energy storage devices. *Inorganic Chemistry Communications*, *115*, 107865–107865. https://doi.org/10.1016/j.inoche.2020.107865

Bajracharya, S., ElMekawy, A., Srikanth, S., & Pant, D. (2016). Cathodes for microbial fuel cells. In K. Scott & E. H. Yu (Eds.), *Microbial Electrochemical and Fuel Cells* (pp. 179–213). Woodhead Publishing. https://doi.org/10.1016/b978-1-78242-375-1.00006-x

Balint, R., Cassidy, N. J., & Cartmell, S. H. (2014). Conductive polymers: Towards a smart biomaterial for tissue engineering. *Acta Biomaterialia*, *10*(6), 2341–2353. https://doi.org/10.1016/j.actbio.2014.02.015

Ref. code: 25666422040920FRA

Beyazıt, N., & Atmaca, K. (2021). COD and Color Removal from Landfill Leachate by photo- electro-Fenton Process. *International Journal of Electrochemical Science*, *16*(5), 210539. https://doi.org/10.20964/2021.05.65

Cheng, S., Liu, W. F., Guo, J. T., Sun, D., Pan, B., Ye, Y., Ding, W., Huang, H., & Li, F. (2014). Effects of hydraulic pressure on the performance of single chamber air-cathode microbial fuel cells. *Biosensors and Bioelectronics*, *56*, 264–270. https://doi.org/10.1016/j.bios.2014.01.036

Choudhury, P., Uday, U. S. P., Mahata, N., Nath Tiwari, O., Narayan Ray, R., Kanti Bandyopadhyay, T., & Bhunia, B. (2017). Performance improvement of microbial fuel cells for waste water treatment along with value addition: A review on past achievements and recent perspectives. *Renewable and Sustainable Energy Reviews*, *79*, 372–389. https://doi.org/10.1016/j.rser.2017.05.098

Corni, I., Ryan, M. P., & Boccaccini, A. R. (2008). Electrophoretic deposition: From traditional ceramics to nanotechnology. *Journal of the European Ceramic Society*, *28*(7), 1353–1367. https://doi.org/10.1016/j.jeurceramsoc.2007.12.011

Deng, Q., Li, X., Zuo, Jiane., Ling, A., & Logan, B. E. (2010). Power generation using an activated carbon fiber felt cathode in an upflow microbial fuel cell. *Journal of Power Sources*, *195*(4), 1130–1135. https://doi.org/10.1016/j.jpowsour.2009.08.092

Dewan, A., Beyenal, H., & Lewandowski, Z. (2008). Scaling up Microbial Fuel Cells. *Environmental Science & Technology*, *42*(20), 7643–7648. https://doi.org/10.1021/es800775d

Dumitru, A., & Scott, K. (2016). Anode materials for microbial fuel cells. In K. Scott & E. H. Yu (Eds.), *Microbial Electrochemical and Fuel Cells* (pp. 117–152). Woodhead Publishing. https://doi.org/10.1016/b978-1-78242-375-1.00004-6

Elakkiya, E., & Matheswaran, M. (2013). Comparison of anodic metabolisms in bioelectricity production during treatment of dairy wastewater in Microbial Fuel Cell. *Bioresource Technology*, *136*, 407–412. https://doi.org/10.1016/j.biortech.2013.02.113

Faria, A., Gonçalves, L., Peixoto, J. M., Peixoto, L., Brito, A. G., & Martins, G. (2017). Resources recovery in the dairy industry: bioelectricity production

Ref. code: 25666422040920FRA

using a continuous microbial fuel cell. *Journal of Cleaner Production*, *140*, 971–976. https://doi.org/10.1016/j.jclepro.2016.04.027

Ghadge, A. N., & Ghangrekar, M. M. (2015). Development of low cost ceramic separator using mineral cation exchanger to enhance performance of microbial fuel cells. *Electrochimica Acta*, *166*, 320–328. https://doi.org/10.1016/j.electacta.2015.03.105

Greenman, J., Gajda, I., You, J., Mendis, B. A., Obata, O., Pasternak, G., & Ieropoulos, I. (2021). Microbial fuel cells and their electrified biofilms. *Biofilm*, *3*, 100057. https://doi.org/10.1016/j.bioflm.2021.100057

Haq, O. ul, Choi, J.-H., & Lee, Y.-S. (2020). Synthesis of ion-exchange polyaniline-carbon composite electrodes for capacitive deionization. *Desalination*, *479*, 114308. https://doi.org/10.1016/j.desal.2019.114308

Huang, L., Chai, X., Cheng, S., & Chen, G. (2011). Evaluation of carbon-based materials in tubular biocathode microbial fuel cells in terms of hexavalent chromium reduction and electricity generation. *Chemical Engineering Journal*, *166*(2), 652–661. https://doi.org/10.1016/j.cej.2010.11.042

Iftimie, S., & Dumitru, A. (2019). Enhancing the performance of microbial fuel cells (MFCs) with nitrophenyl modified carbon nanotubes-based anodes. *Applied Surface Science*, *492*, 661–668. https://doi.org/10.1016/j.apsusc.2019.06.241

Kajama, M. N. (2015). Hydrogen permeation using nanostructured silica membranes. *Sustainable Development and Planning VII*. https://doi.org/10.2495/sdp150381

Kaneda, C., Yuka Sueyasu, Tanaka, E., & Mahito Atobe. (2020). Electrochemical synthesis of microporous polyaniline films using foam templates prepared by ultrasonication. *Ultrasonics Sonochemistry*, *64*, 104991–104991. https://doi.org/10.1016/j.ultsonch.2020.104991

Karmakar, S., Kundu, K., Kundu, S. (2010). Design adn development of microbial fuel cells. Current Research, Technologyand Education Topics in Applied Microbiology and Microbial Technology, 1029-1034.

Kumar, G. G., Zahoor, A., Nahm, K. S., & Xavier, J. S. (2014). Nanotubular MnO_2/graphene oxide composites for the application of open air-breathing

Ref. code: 25666422040920FRA

cathode microbial fuel cells. *Biosensors and Bioelectronics*, *53*, 528–534. https://doi.org/10.1016/j.bios.2013.10.012

Kumar, R., Singh, L., & Zularisam, A. W. (2016). Exoelectrogens: Recent advances in molecular drivers involved in extracellular electron transfer and strategies used to improve it for microbial fuel cell applications. *Renewable and Sustainable Energy Reviews*, *56*, 1322–1336. https://doi.org/10.1016/j.rser.2015.12.029

Kumar, S. S., Kumar, V., Malyan, S. K., Sharma, J., Mathimani, T., Maskarenj, M. S., Ghosh, P. C., & Pugazhendhi, A. (2019). Microbial fuel cells (MFCs) for bioelectrochemical treatment of different wastewater streams. *Fuel*, *254*, 115526. https://doi.org/10.1016/j.fuel.2019.05.109

Li, C., Zhang, L., Ding, L., Ren, H., & Cui, H. (2011). Effect of conductive polymers coated anode on the performance of microbial fuel cells (MFCs) and its biodiversity analysis. *Biosensors and Bioelectronics*, *26*(10), 4169–4176. https://doi.org/10.1016/j.bios.2011.04.018

Liang, P., Wang, J., Xia, X., Huang, X., Mo, Y., Cao, X., & Fan, M. (2011). Carbon nanotube powders as electrode modifier to enhance the activity of anodic biofilm in microbial fuel cells. *Biosensors and Bioelectronics*, *26*(6), 3000–3004. https://doi.org/10.1016/j.bios.2010.12.002

Logan, B. E., Hamelers, B., Rozendal, R., Schröder, U., Keller, J., Freguia, S., Aelterman, P., Verstraete, W., & Rabaey, K. (2006). Microbial Fuel Cells: Methodology and Technology†. *Environmental Science & Technology*, *40*(17), 5181–5192. https://doi.org/10.1021/es0605016

Logan, B., Cheng, S., Watson, V., & Estadt, G. (2007). Graphite Fiber Brush Anodes for Increased Power Production in Air-Cathode Microbial Fuel Cells. *Environmental Science & Technology*, *41*(9), 3341–3346. https://doi.org/10.1021/es062644y

Lu, H., Oehmen, A., Virdis, B., Keller, J., & Yuan, Z. (2006). Obtaining highly enriched cultures of Candidatus Accumulibacter phosphates through alternating carbon sources. *Water Research*, *40*(20), 3838–3848. https://doi.org/10.1016/j.watres.2006.09.004

Ref. code: 25666422040920FRA

Mathew, S., & Thomas, P. C. (2020). Fabrication of polyaniline nanocomposites as electrode material for power generation in microbial fuel cells. *Materials Today: Proceedings*, *33*, 1415–1419. https://doi.org/10.1016/j.matpr.2020.06.502

Mook, W. Y., Aroua, M. K., Chakrabarti, M. H., Noor, I. M., Irfan, M., & Low, C. K. (2013). A review on the effect of bio-electrodes on denitrification and organic matter removal processes in bio-electrochemical systems. *Journal of Industrial and Engineering Chemistry*, *19*(1), 1–13. https://doi.org/10.1016/j.jiec.2012.07.004

Narayanasamy, S., & Jayaprakash, J. (2021). Carbon cloth/nickel cobaltite ($NiCo_2O_4$)/polyaniline (PANI) composite electrodes: Preparation, characterization, and application in microbial fuel cells. *Fuel*, *301*, 121016. https://doi.org/10.1016/j.fuel.2021.121016

Natarajan, S. R. (1985). Current efficiency and electrochemical equivalent in an electrolytic process. *Bulletin of Electrochemistry*, *01*(02), 215–216. http://cecri.csircentral.net/id/eprint/2131

Negassa, L. W., Mohiuddin, M., & Tiruye, G. A. (2021). Treatment of brewery industrial wastewater and generation of sustainable bioelectricity by microbial fuel cell inoculated with locally isolated microorganisms. *Journal of Water Process Engineering*, *41*, 102018. https://doi.org/10.1016/j.jwpe.2021.102018

Pandey, V. K., Verma, S., & Verma, B. (2022). Polyaniline/activated carbon/copper ferrite (PANI/AC/CuF) based ternary composite as an efficient electrode material for supercapacitor. *Chemical Physics Letters*, *802*, 139780. https://doi.org/10.1016/j.cplett.2022.139780

Pant, D., Van Bogaert, G., Porto-Carrero, C., Diels, L., & Vanbroekhoven, K. (2011). Anode and cathode materials characterization for a microbial fuel cell in half cell configuration. *Water Science and Technology*, *63*(10), 2457–2461. https://doi.org/10.2166/wst.2011.217

Park, D. H., & Zeikus, J. G. (2002). Improved fuel cell and electrode designs for producing electricity from microbial degradation. *Biotechnology and Bioengineering*, *81*(3), 348–355. https://doi.org/10.1002/bit.10501

Ref. code: 25666422040920FRA

Peng, L., You, S.-J., & Wang, J.-Y. (2010). Carbon nanotubes as electrode modifier promoting direct electron transfer from Shewanella oneidensis. *Biosensors and Bioelectronics*, *25*(5), 1248–1251. https://doi.org/10.1016/j.bios.2009.10.002

Rabaey, K., Clauwaert, P., Aelterman, P., & Verstraete, W. (2005). Tubular Microbial Fuel Cells for Efficient Electricity Generation. *Environmental Science & Technology*, *39*(20), 8077–8082. https://doi.org/10.1021/es050986i

Rasyad, A., & Budiarto, B. (2018). Analisis Pengaruh Temperatur, Waktu, dan Kuat Arus Proses Elektroplating terhadap Kekuatan Tarik, Kekuatan Tekuk dan Kekerasan pada Baja Karbon Rendah. *Jurnal Rekayasa Mesin*, *9*(3), 173–182. https://doi.org/10.21776/ub.jrm.2018.009.03.4

Rossi, R., & Logan, B. E. (2021). Using an anion exchange membrane for effective hydroxide ion transport enables high power densities in microbial fuel cells. *Chemical Engineering Journal*, *422*, 130150. https://doi.org/10.1016/j.cej.2021.130150

Samsudeen, N., Sharma, A., Radhakrishnan, T. K., & Matheswaran, M. (2015). Performance investigation of multi-chamber microbial fuel cell: An alternative approach for scale up system. *Journal of Renewable and Sustainable Energy*, *7*(4), 043101. https://doi.org/10.1063/1.4923393

Santoro, C., Arbizzani, C., Erable, B., & Ieropoulos, I. (2017). Microbial fuel cells: From fundamentals to applications. A review. *Journal of Power Sources*, *356*, 225–244. https://doi.org/10.1016/j.jpowsour.2017.03.109

Sejati, E. S., & Sudarlin. (2021). The Effect of Multiple Electrode Pairs to Electricity Potential of Ceramic-Based and Tempe Waste Microbial Fuel Cell. *Journal of Physics*, *1788*(1), 012010–012010. https://doi.org/10.1088/1742-6596/1788/1/012010

Shih, Y.-C., Lin, H.-L., & Lin, K.-F. (2017). Electropolymerized polyaniline/graphene nanoplatelet/multi-walled carbon nanotube composites as counter electrodes for high performance dye-sensitized solar cells. *Journal of Electroanalytical Chemistry*, *794*, 112–119. https://doi.org/10.1016/j.jelechem.2017.04.010

Ref. code: 25666422040920FRA

Siagian, K., Arbianti, R., & Utami, T. S. (2017). The influence of biofilm formation on electricity production from tempe wastewater using tubular membraneless microbial fuel cell reactor. *Nucleation and Atmospheric Aerosols*. https://doi.org/10.1063/1.4982263

Sonawane, J. M., Al-Saadi, S., Singh Raman, R. K., Ghosh, P. C., & Adeloju, S. B. (2018). Exploring the use of polyaniline-modified stainless steel plates as low-cost, high-performance anodes for microbial fuel cells. *Electrochimica Acta*, *268*, 484–493. https://doi.org/10.1016/j.electacta.2018.01.163

Strik, D. P. B. T. B., Hamelers, H. V. M., & Buisman, C. J. N. (2010). Solar Energy Powered Microbial Fuel Cell with a Reversible Bioelectrode. *Environmental Science & Technology*, *44*(1), 532–537. https://doi.org/10.1021/es902435v

Sudarlin, S., Afrianto, A. W., Khoerunnisa, M., Rahmadhani, D. W., & Nugroho, A. (2020). Utilization of Montmorillonite-Modified Earthenware from Bentonite-Ca as a Microbial Fuel Cell (MFC) Membrane Based on Tempe Liquid Waste as a Substrate. *Jurnal Kimia Sains Dan Aplikasi*, *23*(6), 222–227. https://doi.org/10.14710/jksa.23.6.222-227

Sun, H., Xu, S., Zhuang, G., & Zhuang, X. (2016). Performance and recent improvement in microbial fuel cells for simultaneous carbon and nitrogen removal: A review. *Journal of Environmental Sciences*, *39*, 242–248. https://doi.org/10.1016/j.jes.2015.12.006

Tamakloe, R. Y., Opoku-Donkor, T., Donkor, M. K. E., & Agamasu, H. (2015). Comparative study of double-chamber microbial fuel cells (DC-MFCs) using Mfensi clay as ion-exchange-partition: Effect of electrodes. *African Journal of Science, Technology, Innovation and Development*, *7*(3), 207–210. https://doi.org/10.1080/20421338.2015.1043706

Thepsuparungsikul, N., Ng, T. C., Lefebvre, O., & Ng, H. Y. (2014). Different types of carbon nanotube-based anodes to improve microbial fuel cell performance. *Water Science and Technology*, *69*(9), 1900–1910. https://doi.org/10.2166/wst.2014.102

Tsai, H.-Y., Wu, C.-C., Lee, C.-Y., & Shih, E. P. (2009). Microbial fuel cell performance of multiwall carbon nanotubes on carbon cloth as electrodes.

Ref. code: 25666422040920FRA

Journal of Power Sources, *194*(1), 199–205. https://doi.org/10.1016/j.jpowsour.2009.05.018

Ucar, D., Zhang, Y., & Angelidaki, I. (2017). An Overview of Electron Acceptors in Microbial Fuel Cells. *Frontiers in Microbiology*, *8*. https://doi.org/10.3389/fmicb.2017.00643

Virdis, B., Read, S. T., Rabaey, K., Rozendal, R. A., Yuan, Z., & Keller, J. (2011). Biofilm stratification during simultaneous nitrification and denitrification (SND) at a biocathode. *Bioresource Technology*, *102*(1), 334–341. https://doi.org/10.1016/j.biortech.2010.06.155

Wang, G., & Feng, C. (2017). Electrochemical Polymerization of Hydroquinone on Graphite Felt as a Pseudocapacitive Material for Application in a Microbial Fuel Cell. *Polymers*, *9*(12), 220. https://doi.org/10.3390/polym9060220

Wang, P., Li, H., & Du, Z. (2014). Polyaniline Synthesis by Cyclic Voltammetry for Anodic Modification in Microbial Fuel Cells. *International Journal of Electrochemical Science*, *9*(4), 2038–2046. https://doi.org/10.1016/s1452-3981(23)07909-9

Wang, X., Feng, Y. J., & Lee, H. (2008). Electricity production from beer brewery wastewater using single chamber microbial fuel cell. *Water Science and Technology*, *57*(7), 1117–1121. https://doi.org/10.2166/wst.2008.064

Wei, J., Liang, P., Cao, X., & Huang, X. (2011). Use of inexpensive semicoke and activated carbon as biocathode in microbial fuel cells. *Bioresource Technology*, *102*(22), 10431–10435. https://doi.org/10.1016/j.biortech.2011.08.088

Winfield, J., Gajda, I., Greenman, J., & Ieropoulos, I. (2016). A review into the use of ceramics in microbial fuel cells. *Bioresource Technology*, *215*, 296–303. https://doi.org/10.1016/j.biortech.2016.03.135

Xiao, L., Damien, J., Luo, J., Jang, H. D., Huang, J., & He, Z. (2012). Crumpled graphene particles for microbial fuel cell electrodes. *Journal of Power Sources*, *208*, 187–192. https://doi.org/10.1016/j.jpowsour.2012.02.036

Xiao, L., Ge, Z., Kelly, P., Zhang, F., & He, Z. (2014). Evaluation of normalized energy recovery (NER) in microbial fuel cells affected by reactor dimensions

Ref. code: 25666422040920FRA

and substrates. *Bioresource Technology*, *157*, 77–83. https://doi.org/10.1016/j.biortech.2014.01.086

Yahampath Arachchige Don, C. D. Y., & Babel, S. (2021). Circulation of anodic effluent to the cathode chamber for subsequent treatment of wastewater in photosynthetic microbial fuel cell with generation of bioelectricity and algal biomass. *Chemosphere*, *278*, 130455. https://doi.org/10.1016/j.chemosphere.2021.130455

Yang, W., Wang, X., Son, M., & Logan, B. E. (2020). Simultaneously enhancing power density and coulombic efficiency with a hydrophobic Fe–N4/activated carbon air cathode for microbial fuel cells. *Journal of Power Sources*, *465*, 228264. https://doi.org/10.1016/j.jpowsour.2020.228264

Yazdi, A. A., D'Angelo, L., Omer, N., Windiasti, G., Lu, X., & Xu, J. (2016). Carbon nanotube modification of microbial fuel cell electrodes. *Biosensors and Bioelectronics*, *85*, 536–552. https://doi.org/10.1016/j.bios.2016.05.033

Yin, T., Zhang, H., Yang, G., & Wang, L. (2019). Polyaniline composite TiO_2 nanosheets modified carbon paper electrode as a high performance bioanode for microbial fuel cells. *Synthetic Metals*, *252*, 8–14. https://doi.org/10.1016/j.synthmet.2019.03.027

You, S., Zhao, Q., Zhang, J., Jiang, J., & Zhao, S. (2006). A microbial fuel cell using permanganate as the cathodic electron acceptor. *Journal of Power Sources*, *162*(2), 1409–1415. https://doi.org/10.1016/j.jpowsour.2006.07.063

You, S.-J. ., Ren, N.-Q. ., Zhao, Q.-L. ., Wang, J.-Y. ., & Yang, F.-L. . (2009). Power Generation and Electrochemical Analysis of Biocathode Microbial Fuel Cell Using Graphite Fibre Brush as Cathode Material. *Fuel Cells*, *9*(5), 588–596. https://doi.org/10.1002/fuce.200900023

Zakir, M., Budi, P., Raya, I., Karim, A., Wulandari, R., & Sobrido, A. B. J. (2018). Determination of specific capacitance of modified candlenut shell based carbon as electrode material for supercapacitor. *Journal of Physics: Conference Series*, *979*, 012024. https://doi.org/10.1088/1742-6596/979/1/012024

Ref. code: 25666422040920FRA

Zhang, F., & He, Z. (2012). Integrated organic and nitrogen removal with electricity generation in a tubular dual-cathode microbial fuel cell. *Process Biochemistry*, *47*(12), 2146–2151. https://doi.org/10.1016/j.procbio.2012.08.002

Zhang, M., Nautiyal, A., Du, H., Wei, Z., Zhang, X., & Wang, R. (2021). Electropolymerization of polyaniline as high-performance binder free electrodes for flexible supercapacitor. *Electrochimica Acta*, *376*, 138037–138037. https://doi.org/10.1016/j.electacta.2021.138037

Zhang, X., Shi, J., Liang, P., Wei, J., Huang, X., Chuan-yi, Z., & Logan, B. E. (2013). Power generation by packed-bed air-cathode microbial fuel cells. *Bioresource Technology*, *142*, 109–114. https://doi.org/10.1016/j.biortech.2013.05.014

Zhang, Y., Mo, G., Li, X., Zhang, W., Zhang, J., Ye, J., Huang, X., & Yu, C. (2011). A graphene modified anode to improve the performance of microbial fuel cells. *Journal of Power Sources*, *196*(13), 5402–5407. https://doi.org/10.1016/j.jpowsour.2011.02.067

Zhong, D., Liao, X., Liu, Y., Zhong, N., & Xu, Y. (2018). Enhanced electricity generation performance and dye wastewater degradation of microbial fuel cell by using a petaline NiO@ polyaniline-carbon felt anode. *Bioresource Technology*, *258*, 125–134. https://doi.org/10.1016/j.biortech.2018.01.117

Zhuang, L., Zeng, R. J., Yueqiang, W., Liu, C., & Geng, S. (2009). Membrane-less cloth cathode assembly (CCA) for scalable microbial fuel cells. *Biosensors and Bioelectronics*, *24*(12), 3652–3656. https://doi.org/10.1016/j.bios.2009.05.032

Zou, Y., Pisciotta, J. M., & Baskakov, I. V. (2010). Nanostructured polypyrrole-coated anode for sun-powered microbial fuel cells. *Bioelectrochemistry*, *79*(1), 50–56. https://doi.org/10.1016/j.bioelechem.2009.11.001

Ref. code: 25666422040920FRA

APPENDICES

Ref. code: 25666422040920FRA

APPENDIX A

UASB SLUDGE SAMPLING

Figure A.1 Sludge sampling at Pathum Thani Brewery, Co., Ltd.

Ref. code: 25666422040920FRA

APPENDIX B

PICTURES OF EXPERIMENTAL MODELS

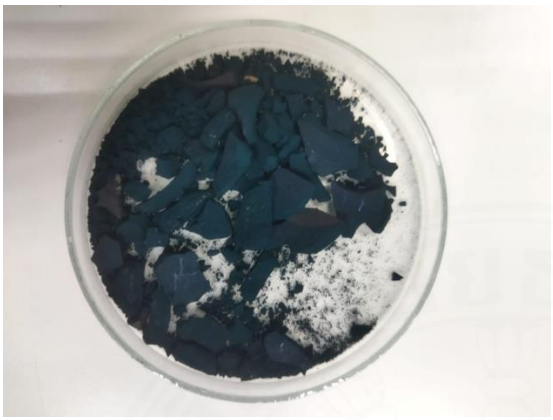

Polyaniline synthesis

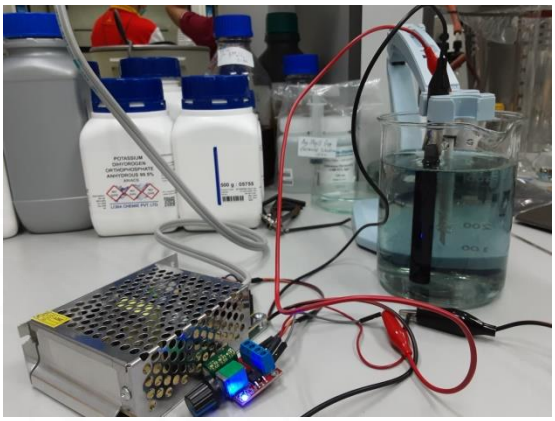

Electrocoating reaction

COD analysis

Figure B.1 Experimental Models

APPENDIX C

MFC SETUP

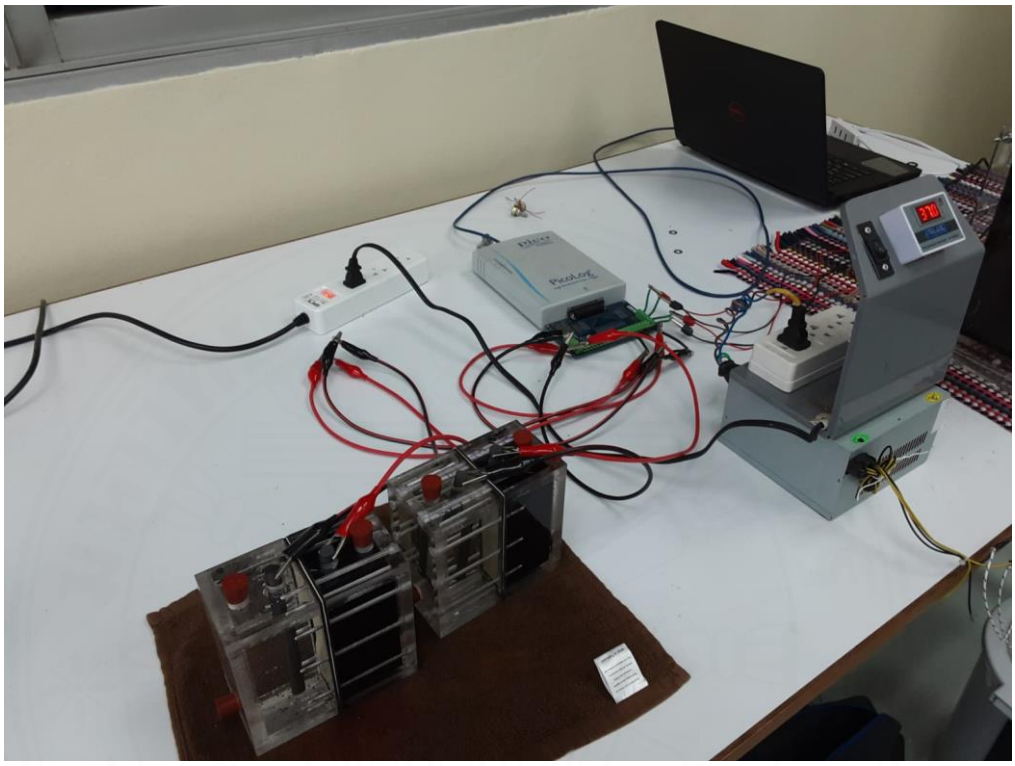

Figure C.1 MFC reactors setup in operational times

Ref. code: 25666422040920FRA

BIOGRAPHY

Name	Andika Wahyu Afrianto
Education	2019: Bachelor of Science (Chemistry), Universitas Islam Negeri Sunan Kalijaga, Yogyakarta, Indonesia
Publications	

Afrianto, A. W., & Babel, S. (2023). Electrode Materials and Their Effects on Electricity Generation and Wastewater Treatment in a Microbial Fuel Cell. In E. Debik, M. Bahadir, & A. Haarstrick (Eds.), *Wastewater Management and Technologies* (pp. 53–72). Springer. https://doi.org/10.1007/978-3-031-36298-9_5

Afrianto, A. W. (2022). Flavonoid Compound from Dichloromethane Extract of Crinum amabile Donn Leaves. *Kaunia: Jurnal Teknosains Dalam Islam*, *18*(1), 17–23. https://doi.org/10.14421/kaunia.3399

Mazlan, Lestari, W. A., Istiqomah, A., Krisdiyanto, D., & **Afrianto, A. W.** (2020). Preparation of Ni/Zeolite as esterification catalyst in biodiesel production based on off-grade crude palm oil. *IOP Conference Series, 858*, 012015–012015. https://doi.org/10.1088/1757-899x/858/1/012015

Sudarlin, S., **Afrianto, A. W.**, Khoerunnisa, M., Rahmadhani, D. W., & Nugroho, A. (2020). Utilization of Montmorillonite-Modified Earthenware from Bentonite-Ca as a Microbial Fuel Cell (MFC) Membrane Based on Tempe Liquid Waste as a Substrate. *Jurnal Kimia Sains Dan Aplikasi*, *23*(6), 222–227. https://doi.org/10.14710/jksa.23.6.222-227

Ref. code: 25666422040920FRA